An effective algorithm for the generation of patient-specific Purkinje networks in computational electrocardiology

Simone Palamara [a], Christian Vergara [b,*], Elena Faggiano [a,c], Fabio Nobile [d]

[a] *MOX, Dipartimento di Matematica, Politecnico di Milano, Italy*
[b] *Dipartimento di Ingegneria Gestionale, dell'Informazione e della Produzione, Università degli Studi di Bergamo, Italy*
[c] *LaBS, Dipartimento di Chimica, Materiali e Ingegneria Chimica "Giulio Natta", Politecnico di Milano, Italy*
[d] *CSQI – MATHICSE, École Polytechnique Fédérale de Lausanne, Switzerland*

Received 14 October 2013
Received in revised form 27 October 2014
Accepted 21 November 2014
Available online 8 December 2014

1. Introduction

The inclusion of the *Purkinje system* in the computational models of the electrical activity of the ventricles is fundamental to obtain accurate and realistic numerical results. Indeed, this system, composed by the Purkinje fibers (PF), provides the electrical signal (the *depolarization wave*) to the ventricular muscle. This allows, in normal conditions, the rapid and coordinate activation of the ventricles [10], and then the correct pumping of the blood flow into the arteries. PF are electrically connected to the ventricular muscle only at certain insertion sites, called Purkinje muscle junctions (PMJ) [18]. From these sites the depolarization wave enters the heart muscle, allowing for the ventricular excitation and contraction [2].

Despite the essential function of PF in the coordinated activation of the ventricles, they have been usually neglected in the computational models. This was mainly due to the difficulty in obtaining *in vivo* images of PF from radiological analyses, since they are excessively thin for the current clinical imaging resolution. For this reason, the inclusion of the PF in the computational models has been often obtained by means of surrogate models such as the definition of space-dependent

* Corresponding author. Tel.: +39 0352052314; fax: +39 0352052310.
E-mail addresses: simone.palamara@polimi.it (S. Palamara), christian.vergara@unibg.it (C. Vergara), elena.faggiano@polimi.it (E. Faggiano), fabio.nobile@epfl.ch (F. Nobile).

conduction muscular properties [23]. There have been, however, some attempts to incorporate PF in the computational models. In particular, three alternatives have been proposed so far to generate a Purkinje network:

i) Segmentation from ex-vivo images [4,26];
ii) A manual procedure based on anatomical knowledge [28,3];
iii) Computational algorithms based on a fractal law [1,12,21].

Among the three alternatives described above, only strategy i) allows to recover patient-specific information on the network, provided that ex-vivo images are available, which is not a common situation. The second and the third strategies are driven only by general anatomical information and therefore do not give the possibility to generate patient-specific networks. Nevertheless, strategy iii) is very appealing from the computational point of view, since it can be easily incorporated in an available code for the simulation of the electrical activity of the heart.

In this work, we adapted strategy iii) to make it patient-specific by using clinical measurements of the electrical activation in the ventricle to locate accurately the PMJ. In particular, we considered the case of an electrical propagation in the muscle originated from sources located on the endocardium. This is a very common situation, occurring for example for a normal propagation or for an ischemic case, where the sources are all identified with the PMJ. The proposed method has been already considered in [29] for an application to three real cases characterized by a normal electrical activity and compared with other strategies proposed so far, obtaining very promising results in terms of accuracy, whereas its extension to pathological situations has been addressed in [17].

In this paper we aimed at describing in detail the proposed method and provide an exhaustive computational study of its accuracy and robustness. To this aim, we applied our method to ideal and real geometries with synthetic measures generated by solving a forward problem, and to a real case with patient-specific clinical measures.

A cross-validation test and the generation of noisy data show that our method is accurate and robust for both geometries. In particular, our method always features a better accuracy in terms of error with the measures with respect to the case of a non-patient-specific Purkinje network.

The outline of the work is as follows. In Section 2 we introduce the mathematical models considered for the computation of the activation times in the ventricle and in the Purkinje network. In Section 3 we detail our method for the generation of a patient-specific Purkinje network in the case of endocardial sources. In Section 4 we show several numerical results in an idealized geometry to highlight the accuracy and the robustness of our method. Finally, in Section 5 we show the application of our algorithm to a real case obtained by considering patient specific geometry and measures, and we simulate an ischemic case.

1.1. A summary of variables and unknowns

We want here to summarize all the variables and unknowns introduced in the text.

$u_m(\boldsymbol{x}), u_e(\boldsymbol{x}), u_p(\boldsymbol{x})$	Activation times in the myocardium, on the endocardium and in the Purkinje network, respectively;
$\Omega_m, \Omega_e, \Omega_p$	Computational domains representing the myocardium, the endocardium and the Purkinje network, respectively;
$\Gamma_m, \Gamma_e, \Gamma_p$	Part of the domain where the boundary conditions representing the source terms are applied in the myocardium, endocardium and Purkinje network, respectively;
V_m, V_e, V_p	Conduction velocity along the muscular fibers in the myocardium, on the endocardium and in the Purkinje network, respectively;
D	Anisotropic tensor accounting for the muscular fibers;
N	Number of measurements;
M	Number of PMJ;
$\boldsymbol{x}_1, \dots, \boldsymbol{x}_N$	Coordinates of the points where the measures were acquired;
$T_1, \dots, T_N$	Measured activation times;
$\boldsymbol{w}_1, \dots, \boldsymbol{w}_M$	Coordinates of the bases of the leaves;
$\boldsymbol{y}_1, \dots, \boldsymbol{y}_M$	Coordinates of the PMJ;
$\tau_1, \dots, \tau_M$	Activation times computed at the PMJ by solving the 1D Eikonal problem in the network;
$t_1, \dots, t_N$	Activation times computed at the measurement points $\boldsymbol{x}_i$ by solving the Eikonal problem on the endocardium or in the myocardium.

2. Modeling the electrical activity

2.1. The electrical activation in the ventricular muscle

2.1.1. The anisotropic 3D Eikonal problem

The algorithm for the generation of a patient-specific Purkinje network we are going to describe in Section 3 is based on the computation of the discrepancy between the measured and the computed activation times, defined as the instant at

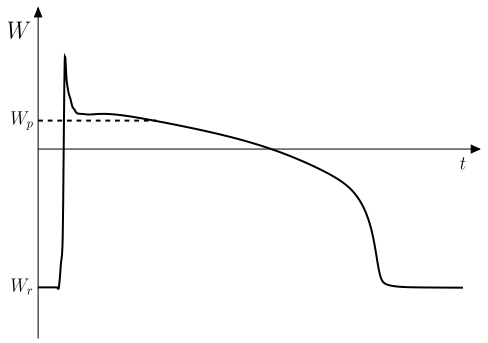

Fig. 1. Characteristic waveform representing the action potential of a heart cell.

which the potential W reaches the value $(W_r + W_p)/2$, where W_r is the minimum value and W_p the value reached at the plateau (see Fig. 1). The activation times could be obtained computationally by solving suitable mathematical models. Classical models for the mathematical description of the electrical activity in the ventricles are the *Bidomain* and the *Monodomain* models [9,14,30,6], which consist in modeling the ventricular tissue as a functional syncytium of electrically coupled cells and in deriving continuous models of reaction–diffusion equations. Such models describe the electrical potential in each point of the ventricle and at each time. As a byproduct, activation times can be computed.

In this work, we decided to consider a simplified model derived from the Bidomain one, suitable when one needs to know only the activation times, that is the *anisotropic Eikonal equation* [13,7]. It describes the activation time in any point of the computational domain, and it has been proved to be a good approximation of the more complex Bidomain one [7]. Such a model is far less expensive in term of computational time than the Bidomain or the Monodomain ones, since it is a steady problem and it does not exhibit an internal or boundary layer as happens when considering such models [7]. Recently, the Eikonal model has been considered also for clinical applications [27].

Let Ω_m be the three-dimensional computational domain related to the muscular propagation and $u_m = u_m(\boldsymbol{x})$ the unknown activation time. Then, the anisotropic Eikonal model reads

$$\begin{cases} V_m \sqrt{(\nabla u_m)^T D \nabla u_m} = 1 & \boldsymbol{x} \in \Omega_m, \\ u_m(\boldsymbol{x}) = u_{m,0}(\boldsymbol{x}) & \boldsymbol{x} \in \Gamma_m, \end{cases} \tag{1}$$

where $V_m = V_m(\boldsymbol{x})$ is the conduction velocity along the muscular fibers in the myocardium (possibly depending on space), $D \in \mathbb{R}^{3\times 3}$ is the anisotropic tensor which accounts for the orientation of the muscular fibers, Γ_m is the set of source points generating the front and $u_{m,0}(\boldsymbol{x})$ is the value of the activation time on Γ_m. For the anisotropic tensor in this work we used the following expression

$$D(\boldsymbol{x}) = k^2 \boldsymbol{I} + \left(1 - k^2\right) \boldsymbol{a}(\boldsymbol{x}) \boldsymbol{a}(\boldsymbol{x})^T, \tag{2}$$

where k is the ratio between the conduction velocity orthogonal to the fibers direction and that along the fibers, and $\boldsymbol{a}$ gives for each point $\boldsymbol{x}$ the unit vector tangential to the fibers [7].

A more complex version of Eq. (1) includes also a diffusion term which accounts for the diffusion process characterizing the front (anisotropic Eikonal-diffusion equation [7]). Such a term describes the relationship between the velocity of propagation and the curvature of the wave-front. However, as a first step in the direction of building patient-specific Purkinje networks, in this work we neglected such a contribution. The validity of such an approximation is supported by the results obtained in [29], where an excellent accuracy has been found when testing our method with real clinical data.

2.1.2. An approximation of the 3D problem: the isotropic Eikonal problem on the endocardium

As described later on, when the sources for the muscular activation are all located on the endocardium, then in our method for the generation of a patient-specific network it will be enough to solve a muscular problem only on the endocardium (see hypothesis H1 in Section 3). Moreover, to simplify the proposed algorithm, for the description of the electrical activity on such a surface, we considered the *isotropic* Eikonal problem. This is of course an approximation, justified by the observation that it is nowadays very hard to have information about the muscular fibers. However, as shown by the numerical experiments reported in Sections 4 and 5, this choice leads to an excellent accuracy. In particular, let Ω_e be the computational domain related to the endocardium and $u_e = u_e(\boldsymbol{x})$ the unknown activation time. Then, the isotropic 2D Eikonal model reads

$$\begin{cases} V_e |\nabla u_e| = 1 & \boldsymbol{x} \in \Omega_e, \\ u_e(\boldsymbol{x}) = u_{e,0}(\boldsymbol{x}) & \boldsymbol{x} \in \Gamma_e, \end{cases} \tag{3}$$

where $V_e = V_e(\boldsymbol{x})$ is the muscular conduction velocity on the endocardium, Γ_e is the set of source points generating the front and $u_{e,0}(\boldsymbol{x})$ is the value of the activation time on Γ_e.

We observe that the velocity V_e in problem (3) should be thought of as a surrogate uniform value of the anisotropic non-uniform endocardial velocity derived from V_m. In our numerical experiments V_e has been determined as the value that best agrees with the measures.

We point out that in accordance with the observations done for the 3D problem, we neglected also in this case the diffusion term.

2.2. The electrical activation in the Purkinje network

To solve problems (1) and (3) we need to provide the boundary conditions $(1)_2$ and $(3)_2$ on Γ_m and Γ_e, respectively, which represent the points where the electrical activation starts. In a normal propagation, Γ_m and Γ_e coincide with the PMJ since the signal traveling along the Purkinje network enters the muscle through these junctions. In particular, we observe that once the electrical signal has reached the PMJ, it enters the ventricle with a delay d_o of about 5–10 ms [11] (anterograde or orthodromic delay).

We then need a mathematical model also to describe the propagation in the Purkinje network. In this respect, it is possible to consider one-dimensional Monodomain [31,22,19] and Bidomain [4] models. In particular, in [19] the effect of the Purkinje network on the cardiac resynchronization therapy has been investigated, whereas in [22] the authors extracted from images information about the morphology of the fibers. However, since we were interested in computing only the activation times in the network (in particular at the PMJ) and not the whole action potential, we considered again the Eikonal equation.

Let Ω_p be the one-dimensional computational domain given by the Purkinje network and $u_p = u_p(\boldsymbol{x})$ the unknown activation time in the network. Then, the Eikonal model reads

$$\begin{cases} V_p \left| \dfrac{\partial u_p}{\partial s} \right| = 1 & \boldsymbol{x} \in \Omega_p, \\ u_p(\boldsymbol{x}) = u_{p,0}(\boldsymbol{x}) & \boldsymbol{x} \in \Gamma_p, \end{cases} \tag{4}$$

where $V_p = V_p(\boldsymbol{x})$ is the conduction velocity (5–10 times greater than the muscular one [15]), s is the curvilinear coordinate, Γ_p is the set of points generating the front (in a normal propagation Γ_p is the atrio-ventricular node) and $u_{p,0}(\boldsymbol{x})$ is the value of the activation time on Γ_p.

We point out that for the modelization of the network, we have considered again the isotropic Eikonal problem. This approximation is perfectly justified due to the absence of muscular fibers (and then of anisotropy) in a 1D network. Again, we neglected the diffusion term since the high advection term V_p dominates any diffusion process.

2.3. Numerical solution of the Eikonal problem

For the solution of the Eikonal problems (1), (3) and (4) we used algorithms belonging to the class of the *Fast Marching Methods* (FMM) [24]. Such methods are based on the observation that the information propagates only from smaller to larger values of the unknown. Based on this, FMM try to follow the front of propagation and at each step three regions are recognized:

1. The *Accepted* region, formed by the points of the domain where the solution has been already determined;
2. The *Trial* region, formed by the points of the domain "close" to the accepted ones and which are potentially new accepted points;
3. The *Far* region, formed by the points of the domain which are far from the accepted ones.

In the classical FMM, at each step of the algorithm the solution is evaluated in the trial points and a new accepted point is created. In particular, in the isotropic case, the Trial region is formed only by the points which are neighbors of the accepted ones and just a single evaluation for each trial point using an upwind scheme is enough to create a new accepted point (*single-pass method*, see [24]). In such a case, the FMM is very efficient, since it follows gradient directions, which coincide with those of propagation (*characteristic directions*). However, in the anisotropic case, the gradient and the characteristic directions do not necessarily coincide and this scheme fails to produce an accurate solution. A possible way to overcome this problem consists in enlarging the Trial region including not only the neighbors but few layers of neighbors, thus allowing the characteristic direction to remain within the neighborhood [25]. This strategy is accurate and single-pass but, in our implementations, it featured a quite high computational time. For this reason, we decided to consider in this work an alternative procedure proposed in [16], where the Trial region is formed by the neighbors solely and a recursive correction is introduced. Such a new step consists in re-computing the value of the unknown in the neighbors of each newly accepted point X, which are inside the Accepted region. This is done since when the values of the unknown have been computed in such neighbors, the value in X had not been used since it was not known. If the new evaluation in a neighbor of X returns a lower value of the unknown with respect to the previous one, then the solution in such a point is updated. This method is not anymore single-pass. However, it uses only the neighbors to compute the value of the unknown in a point, allowing for good performance from the computational point of view (see [16] for further details).

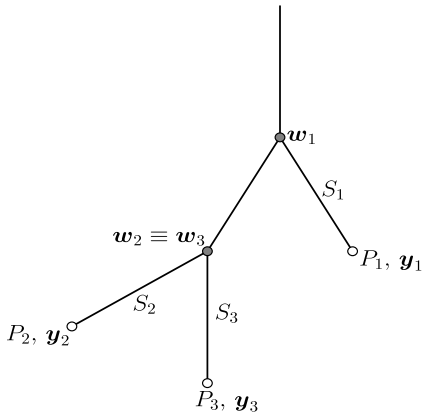

Fig. 2. Structure of the Purkinje network. The grey points are the bases $\boldsymbol{w}_k$ of the leaves S_k, whereas the white points represent the PMJ P_k. In the picture we have $M_{lev} = 2$ and the number of PMJ M is equal to 3.

3. Computational generation of a patient-specific Purkinje network: the case of endocardial sources

In this section we describe the method for the generation of a patient-specific network. In particular, in this work we consider the case of sources for the muscular propagation located only on the endocardium. This is the case for example of a normal electrical propagation or of an ischemic case, where the sources are all located in the PMJ. This means that Γ_m in the 3D Eikonal problem and Γ_e in the 2D one coincide with the PMJ. In such conditions, we can consider the following two simplifying hypotheses:

H1. For the computation of the activation times on the endocardium it is enough to solve an Eikonal problem only on the endocardium. Indeed, if the sources are all located on such a surface, the propagation in the myocardium does not have enough influence on the endocardium. Since for the generation of a patient-specific Purkinje network we only need the endocardial propagation, in our algorithm we solve only problem (3);

H2. The propagation in the PF is not influenced by the muscular propagation, and we can assume that the information propagates uniquely from the Purkinje network towards the muscle cells and that no feedbacks from the muscle are allowed. Therefore, an explicit algorithm could be considered for the numerical solution of the coupled problems (1)–(4) and (3)–(4). In other words, we firstly solved the network solely, and then we used this solution evaluated at the PMJ as sources for the computation of the muscular activation.

We are now ready to describe the method for the generation of the patient-specific Purkinje network. This is composed of two steps: in the first one we generate a *tentative network* by using a fractal law (Section 3.1). In the second step, we update such a network in order to reduce the discrepancy with the clinical measures (Section 3.2).

We give here a description of the structure of a Purkinje network. This is formed by several levels of generation, at each of them we can identify the *active branches* and the *leaves* S_j. An active branch can generate other branches, whereas leaves, starting from the points $\boldsymbol{w}_j$, terminate at their end points $\boldsymbol{y}_j$ which are identified with the PMJ P_j, see Fig. 2.

3.1. Generation of the tentative network

The first tract of the Purkinje network is composed by the *bundle of His*, which starts from the atrio-ventricular node, and by the *main bundle branches*, which are three branches generating from the bundle of His. The starting point of our algorithm consists in manually design the bundle of His and the main bundle branches, accordingly to anatomical a priori knowledge [1,21]. Then, the tentative Purkinje network is generated as a fractal tree. The growing process follows the 'Y' production rule, similar to the one proposed in [1,12,21]. We allow the leaves to be generated after a different number of levels. However, we fix a maximum number of levels of the tree, M_{lev}, tuned in order to have a good covering of all the reachable areas of the endocardium (see Fig. 2).

To ensure a correct distribution of the PMJ on the endocardium, the process of generation of a leaf is governed by a Bernoullian probability law, where the probability to generate a leaf p is a function of the tree level. In particular, we set $p = \sqrt{j/M_{lev}}$, where j is the current level, so that p is small for the first levels and grows in the successive levels. To obtain a more realistic pattern of PF, the lengths of the left branch L_l and of the right branch L_r, and the branching angle α of the new fibers are described by Gaussian variables.

This procedure allows us to generate a tentative Purkinje network $\mathcal{N}^{(t)}$, characterized by $M^{(t)}$ leaves S_k whose bases are located in $\boldsymbol{w}_k$, $k = 1, \ldots, M^{(t)}$, and by the PMJ P_k, $k = 1, \ldots, M^{(t)}$, located at the points with coordinates $\{\boldsymbol{y}_1^{(t)}, \ldots, \boldsymbol{y}_{M^{(t)}}^{(t)}\} =: \mathcal{P}^{(t)}$, see Fig. 2.

Observe that we have not yet used the clinical data, so that this is not a patient-specific network.

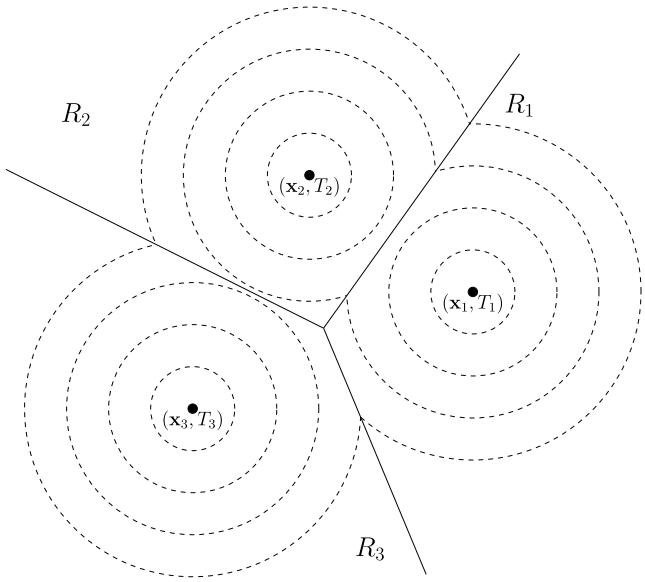

Fig. 3. Regions of influence. Representation of the contour lines of a possible solution of (7) with $N = 3$. The lines represent the points of collision among two or more fronts, and they divide the domain in 3 regions R_i, called regions of influence.

3.2. Generation of the patient-specific network

We describe here the steps to generate a patient-specific network starting from the tentative one $\mathcal{N}^{(t)}$, using clinical measures related to a propagation characterized by endocardial sources solely. Such data are measured on the endocardium, for example before an ablation procedure to burn anomalous propagation sites. This is possible thanks to suitable systems (such as Ensite NavX system, see, e.g., [29]), commonly used nowadays in the clinical practice, which are capable of accurately locating some electrode catheters in the ventricle, allowing for the reconstruction of a map of the activation times [23,27].

In what follows, let $\boldsymbol{x}_i$, $i = 1, \ldots, N$, be the points where the measures have been acquired and T_i the related measured activation times. We summarize the steps related to the generation of the patient-specific network as follows.

Computation of the activation times at the PMJ of $\mathcal{N}^{(t)}$. We solve the 1D Eikonal problem (4) in the tentative network $\mathcal{N}^{(t)}$, by choosing properly the set Γ_p and the boundary condition $u_{p,0}$. For example, for a normal propagation, Γ_p is identified with the atrio-ventricular node. This allows to compute the activation times for all the points of $\mathcal{N}^{(t)}$, and in particular to store the activation times $\tau_k^{(t)} := u_p(\boldsymbol{y}_k^{(t)})$, $k = 1, \ldots, M^{(t)}$, computed at the PMJ.

Construction of the regions of influence. Ideally, the PMJ should be able to describe exactly the observed activation times. In this respect, we say that a set of M sources $(\boldsymbol{z}_k, \zeta_k)$ is *compatible* with the measurements if the following holds:

$$u_e(\boldsymbol{x}_i) = T_i \quad \forall i = 1, \ldots, N, \tag{5}$$

with

$$\begin{cases} V_e \left|\nabla u_e(\mathbf{x})\right| = 1 & \boldsymbol{x} \in \Omega_e, \\ u_e(\boldsymbol{z}_k) = \zeta_k & k = 1, \ldots, M. \end{cases} \tag{6}$$

Notice that, in view of hypothesis H1, we considered the fronts propagating only on the endocardium, thus satisfying the 2D Eikonal problem (3).

To identify such compatible sources, we consider the following *backward Eikonal problem* in the unknown $\tilde{u}_e$:

$$\begin{cases} V_e \left|\nabla \tilde{u}_e(\boldsymbol{x})\right| = 1 & \boldsymbol{x} \in \Omega_e, \\ \tilde{u}_e(\boldsymbol{x}_i) = -T_i & i = 1, \ldots, N. \end{cases} \tag{7}$$

The solution of such a problem divides the domain Ω_e in N regions R_i, called *regions of influence*, which associate to any point $\boldsymbol{x}_i$ the points of the endocardium which could activate $\boldsymbol{x}_i$ at time T_i if used as source points for the muscular propagation. In particular, the boundaries of the regions R_i are identified by the points of collision of two or more fronts propagating from the measurement points $\boldsymbol{x}_i$ (see Fig. 3 for the case $N = 3$).

Exploiting the function $\tilde{u}_e$, we are now able to build a set of M sources that are compatible with the measures. Indeed, let $\mathcal{Z} = \{\hat{\boldsymbol{z}}_1, \ldots, \hat{\boldsymbol{z}}_M\}$ be a set of M points such that at least one point falls in each region R_i, $i = 1, \ldots, N$, or its boundary, and $\mathcal{Z}_i := \{\hat{\boldsymbol{z}}_1^i, \ldots, \hat{\boldsymbol{z}}_{M_i}^i\}$ be the subset of points falling in R_i. Moreover, set

$$\hat{\zeta}_k := -\tilde{u}_e(\hat{\boldsymbol{z}}_k), \quad k = 1, \ldots, M, \qquad \hat{\zeta}_j^i := -\tilde{u}_e\big(\hat{\boldsymbol{z}}_j^i\big), \quad j = 1, \ldots, M_i,\ i = 1, \ldots, N. \tag{8}$$

We have the following result.

Proposition 1. *The M sources $(\hat{\boldsymbol{z}}_k, \hat{\zeta}_k)$, $k = 1, \ldots, M$, defined by (7)–(8) and by $\mathcal{Z}$, are compatible with the measures $(\boldsymbol{x}_i, T_i)$, $i = 1, \ldots, N$, i.e. they satisfy (5)–(6).*

Proof. Given some couples $(\boldsymbol{z}_k, \zeta_k)$, $k = 1, \ldots, M$, the solution in a point $\boldsymbol{x}$ of problem (6) is given by

$$u_e(\boldsymbol{x}) = \min_{l=1,\ldots,M}\left(\zeta_l + \frac{d(\boldsymbol{x}, \boldsymbol{z}_l)}{V_e}\right), \tag{9}$$

where with $d(\cdot, \mathbf{y})$ we have indicated the geodesic distance from $\mathbf{y}$. Then, constraints (5) could be written as follows

$$\min_{l=1,\ldots,M}\left(\zeta_l + \frac{d(\boldsymbol{x}_i, \boldsymbol{z}_l)}{V_e}\right) = T_i \quad i = 1, \ldots, N. \tag{10}$$

Analogously, the solution of problem (7) in a point $\boldsymbol{x}$ is given by

$$\tilde{u}_e(\boldsymbol{x}) = \min_{m=1,\ldots,N}\left(-T_m + \frac{d(\boldsymbol{x}, \boldsymbol{x}_m)}{V_e}\right), \tag{11}$$

and then (8) becomes

$$\hat{\zeta}_k = -\min_{m=1,\ldots,N}\left(-T_m + \frac{d(\hat{\boldsymbol{z}}_k, \boldsymbol{x}_m)}{V_e}\right), \quad k = 1, \ldots, M.$$

In particular, for $\boldsymbol{x} \in R_i$, the expression of (11) is simplified as follows

$$\tilde{u}_e(\boldsymbol{x}) = -T_i + \frac{d(\boldsymbol{x}, \boldsymbol{x}_i)}{V_e}. \tag{12}$$

Now, observing that $\hat{\boldsymbol{z}}_j^i \in R_i$, we have from (12) and (8)

$$\hat{\zeta}_j^i = -\left(-T_i + \frac{d(\hat{\boldsymbol{z}}_j^i, \boldsymbol{x}_i)}{V_e}\right), \quad j = 1, \ldots, M_i. \tag{13}$$

Then, conditions (10) could be written as follows

$$\min_{m=1,\ldots,N}\left(\min_{p=1,\ldots,M_m}\left(\zeta_p^m + \frac{d(\boldsymbol{x}_i, \boldsymbol{z}_p^m)}{V_e}\right)\right) = T_i \quad i = 1, \ldots, N,$$

where ζ_j^m and $\boldsymbol{z}_j^m$ refer to the reordering of ζ_k and $\boldsymbol{z}_k$ following the regions of influence. Then, substituting (13) in the left hand side of the previous expression, we obtain

$$\begin{aligned}
&\min_{m=1,\ldots,N}\left(\min_{p=1,\ldots,M_m}\left(\hat{\zeta}_p^m + \frac{d(\boldsymbol{x}_i, \hat{\boldsymbol{z}}_p^m)}{V_e}\right)\right)\\
&= \min_{m=1,\ldots,N}\left(\min_{p=1,\ldots,M_m}\left(T_m - \frac{d(\hat{\boldsymbol{z}}_p^m, \boldsymbol{x}_m)}{V_e} + \frac{d(\boldsymbol{x}_i, \hat{\boldsymbol{z}}_p^m)}{V_e}\right)\right)\\
&= \min_{m=1,\ldots,N}\left(\min_{p=1,\ldots,M_m}\left(T_m - \frac{d(\hat{\boldsymbol{z}}_p^m, \boldsymbol{x}_m)}{V_e} + \frac{d(\boldsymbol{x}_i, \hat{\boldsymbol{z}}_p^m)}{V_e} - T_i + T_i\right)\right)\\
&= \min_{m=1,\ldots,N}\left(\min_{p=1,\ldots,M_m}\left(-T_i + \frac{d(\boldsymbol{x}_i, \hat{\boldsymbol{z}}_p^m)}{V_e} - \left(-T_m + \frac{d(\hat{\boldsymbol{z}}_p^m, \boldsymbol{x}_m)}{V_e}\right)\right)\right) + T_i = T_i \quad i = 1, \ldots, N,
\end{aligned}$$

where the latter equality holds by noticing that the external minimum is attained for $m = i$, since $-T_m + \frac{d(\hat{\boldsymbol{z}}_p^m, \boldsymbol{x}_m)}{V_e} < -T_i + \frac{d(\boldsymbol{x}_i, \hat{\boldsymbol{z}}_p^m)}{V_e}$ for $m \neq i$ thanks to the analytical solution (12) of the backward problem and to the definition of regions of influence. Therefore, constraints (5) are satisfied and the thesis holds.

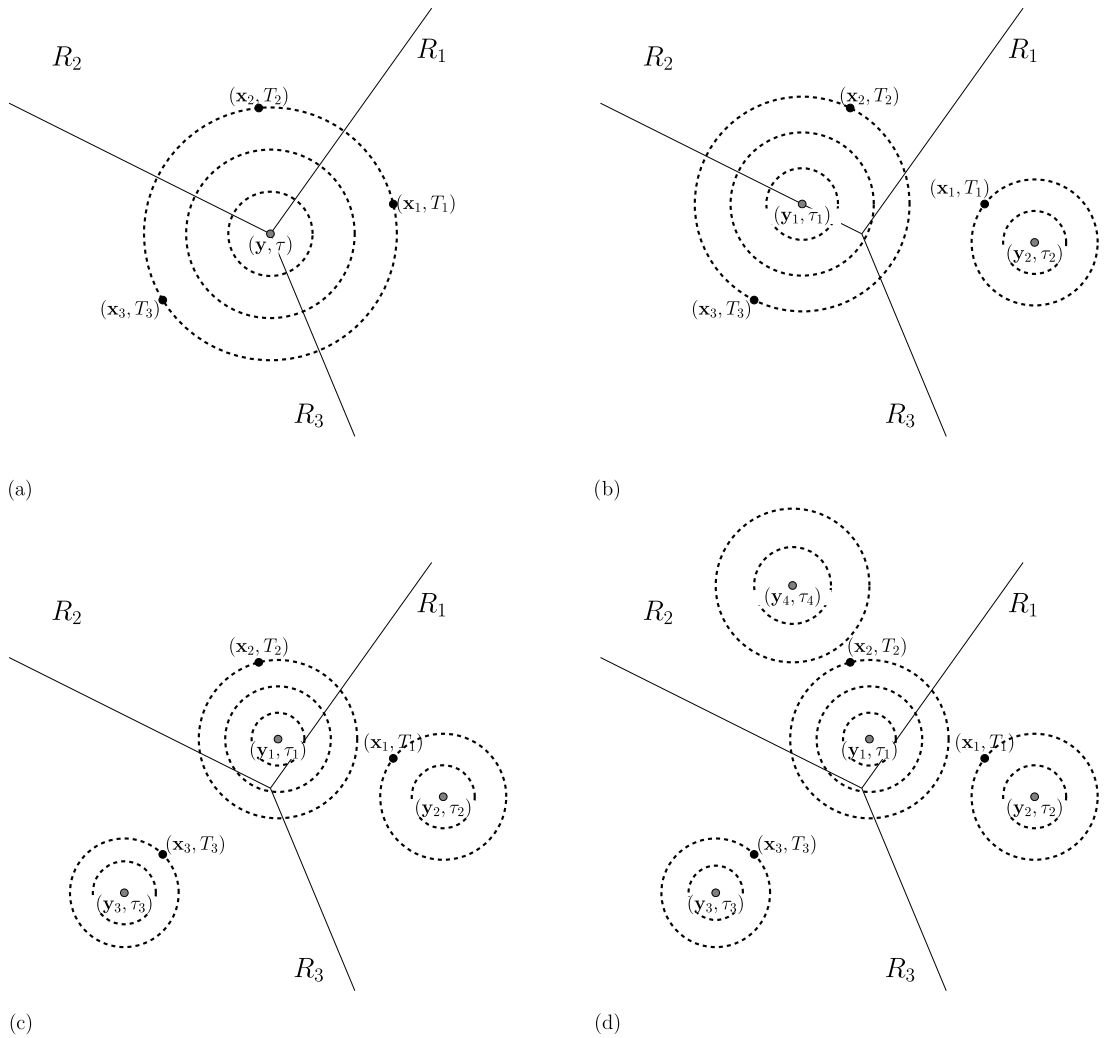

Fig. 4. Examples of possible PMJ configurations. (a) Single PMJ located at the common point of the three regions of influence; (b) two PMJ, one on the boundary between R_2 and R_3, the other one in R_1; (c) three PMJ each one located in a different region; (d) four PMJ, three of them, $\boldsymbol{y}_1, \boldsymbol{y}_2, \boldsymbol{y}_3$, which activate a measure point ($\boldsymbol{x}_1, \boldsymbol{x}_2, \boldsymbol{x}_3$, respectively), and the fourth one, $\boldsymbol{y}_4$, which does not activate any measure point.

Improving the accuracy of the tentative network. Once we have defined the regions of influence R_i, we can identify those of the tentative PMJ belonging to R_i, see Fig. 4. In particular, we introduce for all $i = 1, \ldots, N$ the subsets $\mathcal{P}_i^{(t)} := \{\boldsymbol{y}_1^{(t)i}, \ldots, \boldsymbol{y}_{M_i^{(t)}}^{(t)i}\} \subset \mathcal{P}^{(t)}$ containing the PMJ P_j^i, $j = 1, \ldots, M_i^{(t)}$, belonging to the i-th region of influence R_i. The idea is now to adapt the location of the PMJ of the tentative network so as to improve the accordance with the measures, or possibly make them compatible with the measures. The regions of influence could provide useful indications on how to adapt the PMJ location to the measurements. In particular, an optimal choice would be provided by moving the PMJ in points that satisfy the hypotheses of Proposition 1, that is identifying the coordinates of the PMJ $\boldsymbol{y}_k$ with $\hat{\boldsymbol{z}}_k$, and the related activation times τ_k with $\hat{\zeta}_k$. Indeed, thanks to Proposition 1 this would lead to a set of compatible sources.

Observe however, that the activation time of the PMJ cannot be chosen arbitrarily as it has to be a solution of the 1D Eikonal problem (4). Moreover, we constrained the movement of the PMJ to stay within its region of influence and to be relatively small so that the length of the modified branch is still in the physiological range. Under these constraints there is no guarantee to satisfy exactly the measures. We therefore aim at developing a strategy that improves the tentative network, still fulfilling the above constraints, reducing the discrepancy with the measures. In particular, we look for new positions $\boldsymbol{y}_k$ of the PMJ and for the related activation times $\tau_k = u_p(\boldsymbol{y}_k)$ in an iterative framework, by generating a sequence of networks.

To this aim, we quantify the accuracy of a network by computing the percentage of *satisfied points*. A datum located at $\boldsymbol{x}_i$ is said to be *satisfied* if

$$|\eta_i| \leq \varepsilon, \tag{14}$$

where η_i is given by

$$\eta_i := \frac{t_i - T_i}{|T_i|}, \quad i = 1, \ldots, N, \tag{15}$$

$t_i := u_e(\boldsymbol{x}_i)$, $i = 1, \ldots, N$, being the activation times computed at the measure point $\boldsymbol{x}_i$ by solving the 2D Eikonal problem (3) on the endocardium with the PMJ as boundary points (i.e. $\Gamma_e = \{\boldsymbol{y}_1, \ldots, \boldsymbol{y}_M\}$) and by using the activation times τ_k as boundary condition $u_{e,0}$. Here, we have exploited hypothesis H2 which allows us to use an explicit method to solve the coupled problem given by the interaction between the propagation in the network and in the muscle.

We observe, however, that to check conditions (14) one needs to solve a forward 2D Eikonal problem for each new network generated by the algorithm. To limit the number of 2D problem to solve, we decided instead to use the discrepancy between the backward 2D Eikonal solution evaluated in a PMJ and the related activation time computed by the 1D Eikonal problem on the tentative network. This has the advantage to use the solution of the backward 2D Eikonal problem, which has been already solved to identify the regions of influence.

To this aim, given a measure $\boldsymbol{x}_i$, we introduce the quantities

$$\chi_j^i := \frac{\tau_j^i - (-\tilde{u}_e(\boldsymbol{y}_j^i))}{|T_i|}, \quad j = 1, \ldots, M_i,\ i = 1, \ldots, N, \tag{16}$$

where, accordingly to the definition of the τ_k's, we have set $\tau_j^i = u_p(\boldsymbol{y}_j^i)$, with $\boldsymbol{y}_j^i$ the coordinates of the j-th PMJ belonging to the i-th region of influence R_i. Then, χ_j^i is the discrepancy between the activation time in the PMJ $P_j^i \in \mathcal{P}_i$ obtained by solving the 1D Eikonal problem in the tentative network and the solution of the backward Eikonal problem (7) evaluated in P_j^i, normalized by the measure $|T_i|$, and we check that conditions

$$\left|\chi_j^i\right| \leq \varepsilon \tag{17}$$

hold for all i and j. Now, the question is whether the satisfaction of conditions (17) imply the one of conditions (14). With this respect, we have the following result, which links the behavior of the η_i with the one of the χ_j^i.

Proposition 2. *Let the following conditions hold for all the PMJ in $\mathcal{P}$:*

(i) $\mathcal{P}_i \neq \emptyset$, $i = 1, \ldots, N$;
(ii) $|\chi_j^i| \leq \varepsilon$ $j = 1, \ldots, M_i$, *and* $i = 1, \ldots, N$;
(iii) $\min_{i=1,\ldots,N}(\min_{j=1,\ldots,M_i} \chi_j^i |T_i|) \geq -\varepsilon T_{min}$, *where* $T_{min} := \min_{i=1,\ldots,N} |T_i|$.

Then conditions (14) *are all satisfied, that is* $|\eta_i| \leq \varepsilon$, $i = 1, \ldots, N$.

Proof. From the definition of χ_j^i(16), we can write

$$\tau_j^i = -\tilde{u}_e(\boldsymbol{y}_j^i) + \chi_j^i |T_i|. \tag{18}$$

From (15), we have also that conditions (14) could be written as

$$T_i - \varepsilon|T_i| \leq t_i \leq T_i + \varepsilon|T_i|\ i = 1, \ldots, N. \tag{19}$$

can write the solution of

$$\begin{cases} V_e\left|\nabla u_e(\mathbf{x})\right| = 1 & \boldsymbol{x} \in \Omega_e, \\ u_e(\boldsymbol{y}_j^i) = \tau_j^i & i = 1, \ldots, N,\ j = 1, \ldots, M_i, \end{cases}$$

as follows

$$u_e(\boldsymbol{x}) = \min_{m=1,\ldots,N}\left(\min_{j=1,\ldots,M_m}\left(\tau_j^m + \frac{d(\boldsymbol{x}, \boldsymbol{y}_j^m)}{V_e}\right)\right).$$

Then the activation time t_i at the measurement point $\boldsymbol{x}_i$, can be written as

$$t_i = u_e(\boldsymbol{x}_i) = \min_{m=1,\ldots,N}\left(\min_{j=1,\ldots,M_m}\left(\tau_j^m + \frac{d(\boldsymbol{x}_i, \boldsymbol{y}_j^m)}{V_e}\right)\right). \tag{20}$$

We fix i and we define the following quantities

$$t_j^k := \tau_j^k + \frac{d(\boldsymbol{x}_i, \boldsymbol{y}_j^k)}{V_e}, \quad k = 1, \ldots, N,\ j = 1, \ldots, M_k. \tag{21}$$

We now observe that a measure located in $\boldsymbol{x}_i$ could be activated by a PMJ belonging to $\mathcal{P}_i$ or by a PMJ not belonging to $\mathcal{P}_i$, so that the external minimum in (20) is fulfilled for $m = i$ in the first case and for $m \neq i$ in the second case. Then, from (20), in the first case we have $t_i = t_j^i$ for some $j = 1, \ldots, M_i$, so that conditions (19) become

$$T_i - \varepsilon|T_i| \leq \tau_j^i + \frac{d(\boldsymbol{x}_i, \boldsymbol{y}_j^i)}{V_e} \leq T_i + \varepsilon|T_i|, \tag{22}$$

which, thanks to (18) and (11), could be written as

$$T_i - \varepsilon|T_i| \leq -\min_{m=1,\ldots,N}\left(-T_m + \frac{d(\boldsymbol{y}_j^i, \boldsymbol{x}_m)}{V_e}\right) + \chi_j^i|T_i| + \frac{d(\boldsymbol{x}_i, \boldsymbol{y}_j^i)}{V_e} \leq T_i + \varepsilon|T_i|.$$

Since $\boldsymbol{y}_j^i \in R_i$, then the minimum in the above inequalities is attained again for $m = i$, so that conditions (19) (and then conditions (14)) become

$$-\varepsilon|T_i| \leq -\frac{d(\boldsymbol{y}_j^i, \boldsymbol{x}_i)}{V_e} + \chi_j^i|T_i| + \frac{d(\boldsymbol{x}_i, \boldsymbol{y}_j^i)}{V_e} \leq \varepsilon|T_i|,$$

which are guaranteed if hypothesis (ii) holds.

Regarding the second case, the measure located in $\boldsymbol{x}_i$ is activated by a PMJ not belonging to $\mathcal{P}_i$, let say $\boldsymbol{y}_j^k$, $k \neq i$. Therefore, by observing that inequalities (22) still hold (even if in this case they are not equivalent to conditions (14)), we have

$$t_i = t_j^k < \min_{l=1,\ldots,M_i} t_l^i \leq T_i + \varepsilon|T_i|. \tag{23}$$

Moreover, since $\boldsymbol{y}_j^k \in R_k$, we have from (11)

$$-\tilde{u}_e\big(\boldsymbol{y}_j^k\big) = T_k - \frac{d(\boldsymbol{x}_k, \boldsymbol{y}_j^k)}{V_e} \geq T_i - \frac{d(\boldsymbol{x}_i, \boldsymbol{y}_j^k)}{V_e},$$

so that, owing to (21) and (18) we obtain

$$t_i = t_j^k = -\tilde{u}_e\big(\boldsymbol{y}_j^k\big) + \chi_j^k|T_k| + \frac{d(\boldsymbol{x}_i, \boldsymbol{y}_j^k)}{V_e} \geq T_i - \frac{d(\boldsymbol{x}_i, \boldsymbol{y}_j^k)}{V_e} + \chi_j^k|T_k| + \frac{d(\boldsymbol{x}_i, \boldsymbol{y}_j^k)}{V_e} = T_i + \chi_j^k|T_k|.$$

Then, using hypothesis (iii), we obtain

$$t_i \geq T_i - \varepsilon T_{min} \geq T_i - \varepsilon|T_i|,$$

which, together with (23), guarantees again that conditions (19) (and then (14)) hold true. □

Remark 1. The satisfaction of hypotheses (i) and (ii) in the previous proposition provides a necessary but not sufficient condition for the fulfillment of conditions (14). Observe, however, that if we considered the absolute quantities $\eta_i := t_i - T_i$ and $\chi_j^i := \tau_j^i + \tilde{u}_e(\boldsymbol{y}_j^i)$ instead of (15) and (16), then Proposition 2 holds true even if only hypotheses (i) and (ii) were satisfied. In this case, one needs only to check that the R_i are not empty and that conditions (17) are satisfied to guarantee that all conditions (14) hold true. However, the numerical results performed with this modification, lead to less accurate patient-specific Purkinje network, so that we do not consider this case here.

We are now ready to describe our strategy, which is based on three steps:

1. Move the PMJ;
2. Delete some PMJ;
3. Create new PMJ,

which are described in what follows.

Move the PMJ. This step allows us to obtain a new Purkinje network $\mathcal{N}^{(0)}$ obtained as a correction of the tentative one $\mathcal{N}^{(t)}$ by moving some PMJ according to the measures, so as to improve the percentage of satisfied measurements. In particular, for all $j = 1, \ldots, M_i^{(t)}$ such that $|\chi_j^{(t)i}| \leq \varepsilon$, we do nothing, that is we do not move the corresponding PMJ P_j^i. On the contrary, for all j such that $|\chi_j^{(t)i}| > \varepsilon$, we move the corresponding PMJ P_j^i in order to improve the accordance with the clinical measure, guaranteeing however that new locations are compatible with the Purkinje network, i.e. the new couples $(\boldsymbol{y}_j^{(0)i}, \tau_j^{(0)i})$ satisfy the 1D Eikonal problem (4). The solution of this problem is not unique, so in order to fix a possible solution we considered the following criterion.

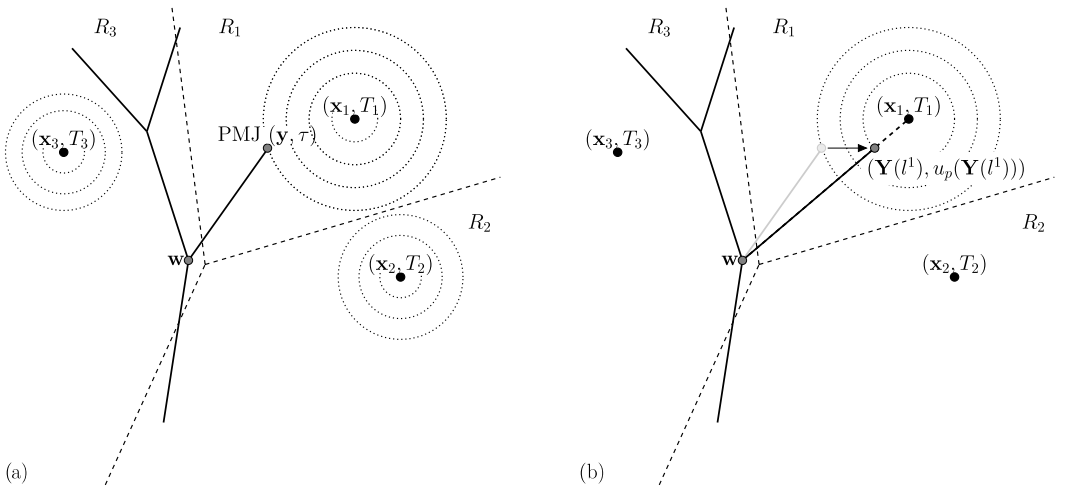

Fig. 5. Moving procedure. The signal propagating in the network activates the PMJ located in $\boldsymbol{y}$ at time τ (a). The PMJ is then moved in the point $\boldsymbol{Y}$, belonging to the straight line joining the base of the leaf $\boldsymbol{w}$ and the measurement point $\boldsymbol{x}_1$, in order to satisfy the measure in $\boldsymbol{x}_i$ according to (26) (b).

Criterion 1. *Given a non-satisfied measure $\boldsymbol{x}_i$, the PMJ P^i_j is located on the geodesic line joining the measure $\boldsymbol{x}_i$ and the base of the leaf related to P^i_j (see Fig. 5).*

In particular, given a point $\boldsymbol{Y} = \boldsymbol{Y}(l)$ on the leaf S^i_j (that is the leaf corresponding to the PMJ P^i_j), with $l \in [l_{min}, l_{max}]$ the local (curvilinear) coordinate related to the geodesic distance and with origin in the base of the leaf, and l_{min} and l_{max} so that the length of the branch is in the physiological range, the solution of the 1D Eikonal problem (4) in $\boldsymbol{Y}$ could be written as follows

$$u_p(\boldsymbol{Y}) = u_p^{ij}(l) := u_p\big(\boldsymbol{w}^i_j\big) + \frac{l}{V_p}, \tag{24}$$

where $\boldsymbol{w}^i_j$ are the coordinates of the root of the leaf S^i_j. On the other side, the solution of the backward 2D Eikonal problem in $\boldsymbol{Y}$ could be written as follows

$$\tilde{u}_e(\boldsymbol{Y}) = \tilde{u}_e^{ij}(l) := -T_i + \frac{L^i_j - l}{V_e}, \tag{25}$$

where $L^i_j := d(\boldsymbol{w}^i_j, \boldsymbol{x}_i)$ is the geodesic distance between the measure located in $\boldsymbol{x}_i$ and the base of the leaf S^i_j. Therefore, by imposing

$$u_p^{ij}(l) = -\tilde{u}_e^{ij}(l),$$

we find the distance from the base of the leaf S^i_j which guarantees that the PMJ P^i_j activates the measure located in $\boldsymbol{x}_i$ and at the same time belongs to the Purkinje network. This leads to the following optimal value

$$l^i_j = \frac{V_p V_e}{V_p - V_e}\left(u_p\big(\boldsymbol{w}^i_j\big) - \left(T_i - \frac{L^i_j}{V_e}\right)\right). \tag{26}$$

We then move accordingly the related PMJ, that is we set $\boldsymbol{Y} = \boldsymbol{Y}(l^i_j)$, guaranteeing $\chi^{(0)i}_j = 0$ if $l^i_j \in [l_{min}, l_{max}]$. If $l^i_j [l_{min}, \notin l_{max}]$, we look for a new $l^i_j \in [l_{min}, l_{max}]$ which minimizes χ^i_j. Owing to (16), (24) and (25), the expression of χ^i_j could be written as follows

$$\chi^i_j(l) = \frac{u_p^{ij}(l) + \tilde{u}_e^{ij}(l)}{|T_i|} = \frac{u_p(\mathbf{w}^i_j) - T_i + \frac{L^i_j}{V_e} + \frac{l(V_e - V_p)}{V_e V_p}}{|T_i|}, \quad j = 1, \ldots, M_i.$$

Since $V_e < V_p$, it is easy to check that $(\chi^i_j(l))' < 0$, so that the minimum of χ^i_j belongs to one of the two extrema l_{min} or l_{max}. Then, we conclude that if $l^i_j < l_{min}$, then we set $l^i_j = l_{min}$, otherwise if $l^i_j > l_{max}$, then we set $l^i_j = l_{max}$. In both cases, we observe that we have $\chi^{(0)i}_j \neq 0$.

At the end of the moving procedure, we have obtained a new Purkinje network $\mathcal{N}^{(0)}$ characterized by $M^{(0)}$ PMJ. Observe that $M^{(0)} = M^{(t)}$.

Delete damaging PMJ. After the moving procedure, we have the following cases:

1. $\chi_j^{(0)i} = 0$ for all j and i; this means that all l^i_j given by (26) lie in the interval $[l_{min}, l_{max}]$.
2. $\chi_j^{(0)i} \neq 0$ for some j and i; this means that l^i_j given by (26) does not lie in the interval $[l_{min}, l_{max}]$.

In the first case, all the hypotheses of Proposition 2 are satisfied. This implies that all conditions (14) hold true, in particular it is possible to prove that $\eta_i^{(0)} = 0$ for all i. Then, the algorithm ends and $\mathcal{N}^{(0)}$ is the final patient-specific network.

Otherwise, in the second case Proposition 2 tells us that it could happen that $|\eta_s^{(0)}| \geq \varepsilon$ for some s (in general we do not have necessarily $s = i$), even if $0 < |\chi_j^{(0)i}| \leq \varepsilon$, either because some region of influence R_s could be empty (hypothesis (i) in Proposition 2 not satisfied), or because hypothesis (iii) in Proposition 2 is not satisfied. Then, we are not still guaranteeing that all conditions (14) are satisfied and we have to modify the network $\mathcal{N}^{(0)}$.

To this aim, we allow the algorithm to delete some PMJ and to create new ones. We firstly delete the so-called "damaging" PMJ, that is those which avoid the satisfaction of the measures. In particular, we notice that $|\eta_i| \geq \varepsilon$ could be given either because $\eta_i \leq -\varepsilon$ or because $\eta_i \geq \varepsilon$. In the first case ($\eta_i \leq -\varepsilon$) we do not have any chance to create a new PMJ producing a smaller error, without deleting the PMJ $\widetilde{P}$ responsible of the activation in $\boldsymbol{x}_i$. Indeed, the signal produced by the new PMJ would be i) either in late with respect to the signal generated by $\widetilde{P}$, and thus without the possibility of activating $\boldsymbol{x}_i$, ii) or early with respect to the signal generated by $\widetilde{P}$, thus activating $\boldsymbol{x}_i$ but, precisely for this reason, producing a bigger error.

In what follows we explain in the detail the delete procedure. Let P_q for some $q = 1, \ldots, M^{(0)}$, be the PMJ which activates $\boldsymbol{x}_i$. We have to distinguish three situations:

1. $\eta_i \leq -\varepsilon$, $P_q \in \mathcal{P}_i$. In this case, the datum in $\boldsymbol{x}_i$ is activated by a PMJ belonging to R_i and the signal arrives early with respect to the measure. Then, we have not any chance to satisfy this datum since whatever movement of P_q would produce a bigger error (remember that P_q is in the optimal site with respect to Criterion 1). Moreover, we do not have any hope to satisfy the datum in $\boldsymbol{x}_i$ by moving another PMJ or by creating new leaves since to produce a smaller error, the signal should be in late with respect to that produced by P_q and therefore it could not activate the point $\boldsymbol{x}_i$. Then, it is impossible to satisfy the datum in $\boldsymbol{x}_i$ so that we delete PMJ P_q. This makes it possible to create a new PMJ which could satisfy the datum (see below);
2. $\eta_i \leq -\varepsilon$, $P_q \notin \mathcal{P}_i$. In this case, the datum in $\boldsymbol{x}_i$ is activated by P_q lying in another region of influence and the signal arrives early with respect to the measure. We can in principle move P_q to reduce the error with respect to the measure in $\boldsymbol{x}_i$ since the location of P_q is not optimal with respect to $\boldsymbol{x}_i$. However, we observe that P_q could be optimal with respect to another datum $\boldsymbol{x}_s$ for some $s \neq i$. Then, any movement of P_q lead to the loss of optimality with respect to $\boldsymbol{x}_s$, so that again we do not consider any movement of P_q. Moreover, as in the previous case, the movement of another PMJ or the generation of a new PMJ are useless to satisfy the datum $\boldsymbol{x}_i$, which is then impossible to be satisfied. Therefore, we need to delete P_q, even if with this choice the datum $\boldsymbol{x}_s$ will be not in principle satisfied. However, this makes possible to create new PMJ which satisfy the two data $\boldsymbol{x}_i$ and $\boldsymbol{x}_s$ (see below);
3. $\eta_i \geq \varepsilon$. In this case, the signal is in late with respect to the measure. Then, independently of the fact that P_q belongs or not to $\mathcal{P}_i$, any movement of P_q, according to Criterion 1, is useless, since P_q has been located in the optimal site. However, in this case we do not need to delete P_q anymore, since this does not avoid to create new PMJ activating $\boldsymbol{x}_i$. Indeed, a new PMJ, if suitably located, could be able to produce a signal which is early with respect to the one propa-gating from P_q. Then, in this case we would be able to decrease the error. Therefore, since the presence of P_q does not avoid the generation of a new PMJ satisfying the datum, we decide to leave P_q in its original position.

Thanks to this classification, we can now describe the delete procedure. In particular, we introduce iterations until the following criterion is satisfied

$$\eta_i^{(l)} \geq -\varepsilon \quad \forall i = 1, \ldots, N. \tag{27}$$

At each iteration l, we first compute the activation times $\tau_k^{(l)}$ in all the P_k. These values could be obtained owing to (24), thus avoiding the solution of the 1D Eikonal problem (4). We then solve the 2D Eikonal problem (3) on the endocardium by using the PMJ of $\mathcal{N}^{(l)}$ as boundary points (i.e. $\Gamma_e = \{\boldsymbol{y}_1^{(l)}, \ldots, \boldsymbol{y}_{M^{(l)}}^{(l)}\}$) and by using the new activation times $\tau_k^{(l)}$ as boundary condition $u_{e,0}^{(l)}$. This allows to obtain the new computed activation times $t_i^{(l)}$, $i = 1, \ldots, N$, at the measurement points, to compute the new values of the discrepancies $\eta_i^{(l)}$ owing to (15), and then to identify the points $\boldsymbol{x}_i$ such that (27) is not satisfied. For each of such points, we delete accordingly the PMJ responsible for its activation, so that a new network $\mathcal{N}^{(l+1)}$ is obtained.

We observe that this procedure terminates in a finite number of iterations, let say K, allowing to produce the network $\mathcal{N}^{(K)}$ with a positive number of PMJ.

Remark 2. Notice that in the delete procedure we have to solve a 2D Eikonal problem at each iteration. Observe, however, that the number of iterations in such a step is very small with respect to the one we would have in the moving procedure if we checked conditions (14) instead of (17).

Create new PMJ. At the end of the *delete* procedure we are not guaranteeing that all conditions (14) are satisfied. Indeed, for some $\boldsymbol{x}_i$ we could have $\eta_i^{(K)} \geq \varepsilon$. In this case, we consider the part of $\mathcal{N}^{(K)}$ belonging to R_i. We select a point $\boldsymbol{w}^i_{M_i^{(K)}+1}$ on such a portion of the network and we create a new leaf $S^i_{M_i^{(K)}+1}$ lying on the geodesic line joining this point and $\boldsymbol{x}_i$. We then compute the optimal location $l^i_{M_i^{(K)}+1}$ given by (26). If $l^i_{M_i^{(K)}+1} \in [l_{min}, l_{max}]$, then we leave the new PMJ in such a position which guarantees $\chi^{(K+1)i}_{M_i^{(K+1)}} = 0$. We observe that in this case we can infer that $\eta_i^{(K+1)} = 0$, since the other PMJ, thanks to the delete procedure, generate fronts which arrive in any case in late, so that they cannot influence the activation in $\boldsymbol{x}_i$. If $l^i_{M_i^{(K)}+1} \notin [l_{min}, l_{max}]$, we then delete such a leaf and we repeat this procedure by considering another point $\boldsymbol{w}^i_{M_i^{(K)}+1}$. At the end of such a procedure we will have obtained our final network $\mathcal{N}^{(K+1)}$ which allowed us to obtain a better accuracy with respect to the tentative network.

The overall sequence of steps is presented in Algorithm 1.

Algorithm 1 Generation of patient-specific Purkinje network – endocardial sources.

Given the vector of the measures `T` in the points defined by the vector `X`, the conduction velocities `V_p` and `V_e`, the extrema `L_min` and `L_max`, the tolerance `EPS`, the tentative network `NET` and in particular the position of the PMJ `Y`, perform the following steps

```
Solve the 1D Eikonal problem (4) in NET;
Solve the backward Eikonal problem (7);
Define the regions of influence R_i;
FOR i=1:N
    FOR j=1:M_i
        Compute the optimal location L with (26);
        IF (L < L_min) THEN L = L_min;
        ELSEIF (L > L_max) THEN L = L_max;
        END IF
        Move the PMJ: Y[i,j] -> Y[i,j] according to (26);
        NET -> NET;
    END FOR
END FOR
Solve the Eikonal problem (3) with NET as sources;
Compute the errors ETA with (15);
Build the vector Z containing the PMJ activating X;
WHILE (MIN(ETA) < -EPS) DO
    FOR i=1:N
        IF (ETA[i] < -EPS) THEN Delete Z[i];
            NET -> NET;
        END IF
    END FOR
    Solve the Eikonal problem (3) with NET as sources;
    Compute the errors ETA with (15);
    Build the vector Z containing the PMJ activating X;
END WHILE
FOR i=1:N
    IF (ETA[i] > EPS) THEN Create a new leaf owing to (26);
END FOR
```

Remark 3. We observe that in principle our algorithm is not able to produce a network such that $|\eta_i| \leq \varepsilon$, $\forall i$. Indeed, in the *create* procedure the part of $\mathcal{N}^{(K)}$ belonging to R_i could be empty for some i. In this case we do not have any chance to satisfy the datum $\boldsymbol{x}_i$.

Remark 4. We observe that the network obtained by our method depends on the starting tentative network, which is randomly generated with Gaussian and Bernoullian variables, and on some parameters, i.e. the mean value of the length and angles of the branches, the tolerance to identify the satisfied points, and the conduction velocities. Once the tentative network and these parameters have been chosen, the solution generated by our algorithm after the moving and delete procedures is unique, that is the method generates always the same network. Instead, we notice that the "create" procedure produces different networks depending on the order followed to sweep the non-satisfied points.

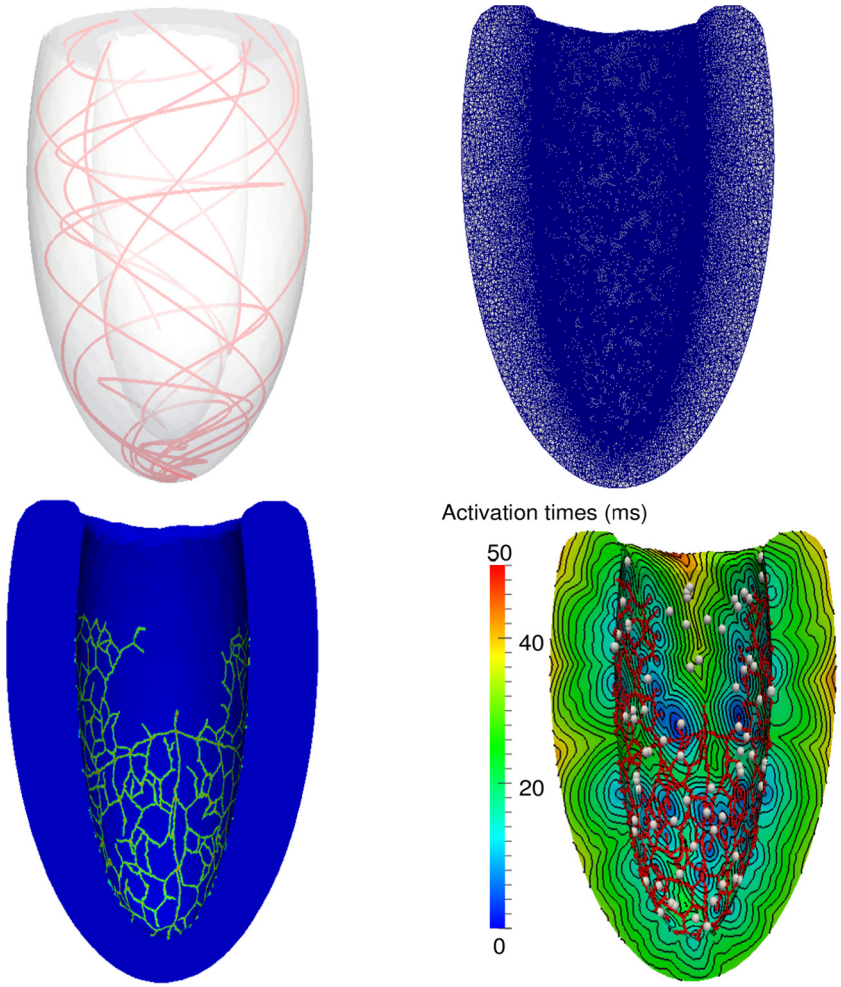

Fig. 6. Procedure for the generation of the synthetic data. Up-left: reconstructed geometry and muscular fibers; up-right: mesh discretization. Bottom-left: reference Purkinje network used in the generation of the synthetic data; bottom-right: activation maps obtained by solving the 3D Eikonal problem (1) with the reference network. The sample $\mathcal{S}$ is represented by grey dots.

4. Numerical results in an idealized geometry

4.1. Physical and numerical specifications

In this section we present several numerical results performed to test the reliability and the robustness of the proposed method for the generation of a patient-specific Purkinje network. To this aim we consider an idealized ventricular geometry given by the ellipsoidal model described in [8], characterized by a set of packed ellipsoidal surfaces, where the length of the semi-principal axes of the inner and outer ellipsoid are $a_x = a_y = 1.5$ cm, $a_z = 4.4$ cm and $b_x = b_y = 2.7$ cm, $b_z = 5$ cm, respectively (see Fig. 6(up-left). To define the anisotropic tensor D by (2), we used the unit vectors tangent to the fibers proposed in [8], and we set $k = 0.46$ [15]. The resulting mesh is composed of about $4 \cdot 10^6$ tetrahedra and $6.4 \cdot 10^5$ vertices, see Fig. 6(up-right). The corresponding endocardial triangular mesh is composed of about $1.45 \cdot 10^5$ elements and $7.3 \cdot 10^4$ vertices.

Since the proposed method is valid only for endocardial sources (see hypotheses H1 and H2) we considered here only normal propagations where the unique source for the network was the atrio-ventricular node and the unique sources for the muscle were the PMJ. In all the numerical tests of this section and of Section 5, unless explicitly stated otherwise, we set $M_{lev} = 30$ determined so as to guarantee that the leaves generation has reached all the regions of interest; $\varepsilon = 10\%$, $d_o = 10$ ms [11]; $l_{min} = h$, with h the space discretization parameter, $l_{max} = l^i_{j,max} = \min\{0.525; L^i_j\}$ so as to guarantee that the lengths of the leaves are into the physiological range; $L_r L_l \sim \mathcal{G}(0.35\text{ cm}, 0.01\text{ cm})$ [21]; $\alpha \sim \mathcal{G}(60°, 1.8°)$ [21], where $\mathcal{G}(\mu, \xi)$ is a Gaussian distribution with mean μ and standard deviation ξ. Moreover, in this section we set $V_p = 3.4$ m/s, $V_m = 0.65$ m/s [15], whereas regarding the conduction velocity on the endocardium V_e in problem (3), we have chosen every time its value with a trial-and-error strategy so as to maximize the accordance with the measures, and guaranteeing

that it falls in the physiological range [15]. Other, more sophisticated strategies could be considered as well, see for example [5] where an optimization procedure has been proposed.

4.2. Validation protocol

In order to validate our algorithm, we need a set of data of activation times on the endocardium. To generate this set of data, we considered a *reference* Purkinje network. This has been built by considering a different realization of the procedure used to generate the fractal tentative network. Of course, due to the randomness of the parameters involved, the reference network is in principle different from the tentative one. Then, we generated a *reference* map of activation times by solving the forward 3D problem (1) with the reference Purkinje network, see Fig. 6(bottom left and right). Finally, the data have been created by sampling N points of the reference map on the endocardium (see Fig. 6(bottom-right)). Due to the procedure used for their generation, we refer to these data as *synthetic*. This allows us to obtain the set of synthetic data $\mathcal{S} := \{(\boldsymbol{x}_1, T_1), \ldots, (\boldsymbol{x}_N, T_N)\}$, where T_i corresponds to the solution of the Eikonal problem (1), with the reference Purkinje network as source term, evaluated in the point $\boldsymbol{x}_i$.

We assessed then the accuracy of the tentative and of the patient-specific networks by comparing the corresponding results with the synthetic data. In particular, let t_i^T, $i = 1, \ldots, N$, be the activation times in the measurement points $\boldsymbol{x}_i$, $i = 1, \ldots, N$, obtained by solving the 3D problem (1) with the tentative network. Analogously, let t_i^P, $i = 1, \ldots, N$, be the activation times in the measurement points $\boldsymbol{x}_i$, $i = 1, \ldots, N$, obtained by solving the 3D problem (1) with the patient-specific network. Then, we computed the mean absolute errors

$$E(\boldsymbol{t}^\beta) := \frac{1}{N}\sum_{i=1}^{N}|t_i^\beta - T_i|, \quad \beta = T, P, \tag{28}$$

and the related standard deviations

$$\sigma(\boldsymbol{t}^\beta) := \sqrt{\frac{1}{N}\sum_{i=1}^{N}|t_i^\beta - T_i|^2 - E^2}, \quad \beta = T, P. \tag{29}$$

4.3. Consistency test

This test has been proposed to prove the ability of our method to generate an accurate Purkinje network. In particular, we considered a sample $\mathcal{S}$ composed by $N = 150$ measurements well-distributed on the endocardium. We notice that the starting point of our algorithm is the tentative network, which is generated randomly according to the Gaussian variables describing the length and the angle of the branches and to the Bernoullian variable describing the probability to generate a PMJ, see Section 3.1. Therefore, a consistency test should prove also the robustness of the method with respect to the tentative network and asses the variability of the results due to the randomness in the generation of the tentative network. To do this, we ran 20 times our algorithm using the same synthetic data but different (randomly generated) tentative networks. Accordingly, to assess the accuracy of the method, we have reported the average over the 20 simulations of the mean absolute errors E^j namely

$$\widehat{E} := \frac{1}{20}\sum_{j=1}^{20}E^j, \quad E^j := \frac{1}{N}\sum_{i=1}^{N}|t_i^j - T_i|, \quad j = 1, \ldots, 20, \tag{30}$$

where t_i^j is the computed activation time at point $\boldsymbol{x}_i$ for the j-th numerical experiment. Regarding the standard deviation, we have to separate the spatial variability from that produced by the repetition of the experiment. In particular, the *mean spatial standard deviation* is defined by

$$\sigma_{sp} := \frac{1}{20}\sum_{j=1}^{20}\sigma^j, \quad \sigma^j = \sqrt{\frac{1}{N}\sum_{i=1}^{N}|t_i^j - T_i|^2 - \left(E^j\right)^2} \tag{31}$$

where σ^j is the spatial standard deviation related to the j-th experiment, whereas the *mean standard deviation over the experiments* is given by

$$\Sigma := \frac{1}{N}\sum_{i=1}^{N}\Sigma_i, \tag{32}$$

where Σ_i is the standard deviation in the point $\boldsymbol{x}_i$ over the 20 numerical experiments, and is defined by

$$\Sigma_i := \sqrt{\frac{1}{20}\sum_{j=1}^{20}|t_i^j - T_i|^2 - (E_i)^2}, \quad E_i := \frac{1}{20}\sum_{j=1}^{20}|t_i^j - T_i|.$$

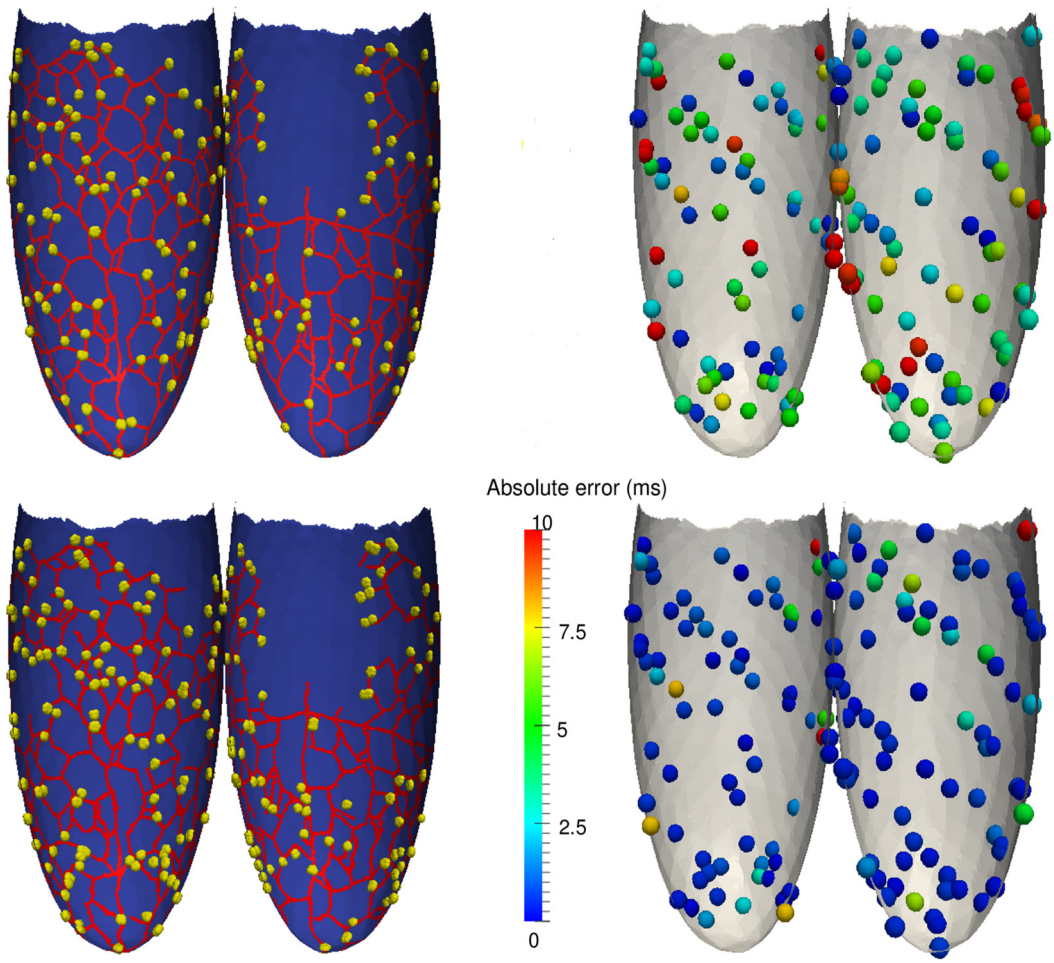

Fig. 7. Left: Purkinje networks (a selected case over the 20). The PMJ are represented by the yellow spheres. Right: absolute errors at the measurement points. Up: tentative network. Bottom: related patient-specific network generated by our method. Consistency test, idealized geometry. (For interpretation of the references to color in this figure legend, the reader is referred to the web version of this article.)

To quantify the total standard deviation, we also introduced the quantity

$$\hat{\sigma} := \sqrt{\frac{1}{20}\sum_{j=1}^{20}\frac{1}{N}\sum_{i=1}^{N}\left|t_i^j - T_i\right|^2 - \widehat{E}^2}. \tag{33}$$

For the experiments reported in this section we also reported the maximum absolute error averaged over the 20 simulations

$$E_{max} := \frac{1}{20}\sum_{j=1}^{20}\Big(\max_{i=1,\dots,N}\left|t_i^j - T_i\right|\Big) \tag{34}$$

and the corresponding standard deviation

$$\sigma_{max} := \sqrt{\frac{1}{20}\sum_{j=1}^{20}\Big(\max_{i=1,\dots,N}\left|t_i^j - T_i\right|\Big)^2 - E_{max}^2}. \tag{35}$$

The best value of the conduction velocity has been found to be $V_e = 0.36$ m/s. The mean number of PMJ were $M^{(t)} = 134.4 \pm 7.4$ for the tentative networks, and $M^{(K+1)} = 193.0 \pm 11.0$ for the patient-specific networks.

In Fig. 7 we depicted a selected tentative network among the 20 we have generated, and the corresponding patient-specific Purkinje network obtained with our method (left) and the absolute errors at the sample $\mathcal{S}$ (right). We observed a qualitative good improvement in the accuracy obtained by using the patient-specific network with respect to that obtained with the tentative one.

Table 1
Mean absolute error $\widehat{E}$ given by (30) and standard deviations σ_{sp}, Σ, and $\hat{\sigma}$ given by (31), (32), and (33), respectively (in ms), obtained by using the tentative and the patient-specific Purkinje networks. The results have to be intended as the average over the 20 simulations. Consistency test, idealized geometry.

Network	$\widehat{E}$	σ_{sp}	Σ	$\hat{\sigma}$
Tentative	3.92	3.10	2.30	3.18
Patient-specific	1.76	2.26	1.47	2.30

Table 2
Maximum absolute error E_{max} given by (34) and standard deviation σ_{max} given by (35) (in ms) obtained by using the tentative and the patient-specific Purkinje networks. The results have to be intended as the average over the 20 simulations. Consistency test, idealized geometry.

Network	E_{max}	σ_{max}
Tentative	17.33	4.09
Patient-specific	12.67	3.15

Table 3
Percentage of satisfied measures obtained by using the tentative and the patient-specific Purkinje networks. The results have to be intended as the average over the 20 simulations. Consistency test, idealized geometry.

Network	Satisfied measures (%)
Tentative	31.1 ± 4.1
Patient-specific	70.2 ± 2.7

Table 4
Mean absolute error E given by (28) and standard deviation σ given by (29) (in ms) obtained with respect to different testing sets with variable size N (the training set being in all the cases formed by 300 points). Cross-validation test, idealized geometry.

N	Tentative	Patient specific
300	3.74 ± 2.83	1.92 ± 2.00
600	3.38 ± 2.76	2.75 ± 2.64
3000	3.52 ± 2.74	2.89 ± 2.79
10 000	3.63 ± 2.84	2.94 ± 2.82

In Table 1 we compared quantitatively the accuracy of the results obtained by using the patient-specific networks generated by our method with that obtained by considering the tentative networks. In both cases, we reported the mean absolute error $\widehat{E}$ and the standard deviations. For the sake of completeness, in Table 2 we reported the spatial maximum absolute error E_{max} and the related standard deviation σ_{max}.

From these results, we noticed a significant improvement of the accuracy obtained by using the patient-specific network with respect to the tentative one. We also observed the small standard deviations for the case of the patient-specific network, even smaller than those related to the tentative network. Moreover, both for the tentative and for the patient-specific networks we obtained that the mean spatial standard deviation σ_{sp} is greater than the mean standard deviation over the experiments Σ. From the last two observations, we then conclude that the proposed algorithm is robust with respect to the choice of the starting network. For this reason, from now on we consider only one run of our algorithm to generate the patient-specific network, so that we report only the usual standard deviation σ given by (29).

Remark 5. As observed in Remark 3, our algorithm in principle does not guarantee that all the measures are satisfied in the sense of (14)–(15). However, we expected that the number of satisfied points should increase with respect to the tentative network. This is the case of all the numerical experiments reported in this paper. Just to provide an example, we reported in Table 3 the percentage of satisfied measures for the consistency test, showing a great improvement when passing from the tentative to the patient-specific network.

4.4. Cross-validation test

In this section we considered a cross-validation test. In particular, we divided the measures in two sets, one used to generate the patient-specific Purkinje network (the *training set*), and another one to validate the network (the *testing set*), given by the remaining points. In particular, we considered a sample $\mathcal{S}$ of variable size $N \geq 300$ measures well distributed and we have used a training set always composed by 300 points. The location of the measures in the training set was randomly chosen according to a uniform probability function. The best value of the conduction velocity has been found to be $V_e = 0.36$ m/s.

In Table 4 we reported the mean absolute error and the standard deviation obtained by using the patient-specific and the tentative networks for different values of N.

As expected, the numerical results proved that the accuracy obtained by using the tentative network were almost the same for different values of N, whereas that obtained by using the patient-specific network deteriorated for decreasing values of measures used to generate the network. Nevertheless, the performance of the patient-specific network, even in the case when only 3% of the measures were used to drive the generation, were still superior to the tentative one. This clearly showed the improvement in the accuracy of the network when using clinical data, justifying the effort needed to generate a patient-specific network.

In the following tests, we considered all the measures to generate the patient-specific network.

4.5. Robustness test with respect to the samples' distribution

In this section we analyzed the robustness of the proposed method with respect to an unbalanced distributions of the synthetic data. This is the case when the clinicians are not able to reach with the catheters some regions of the endocardium

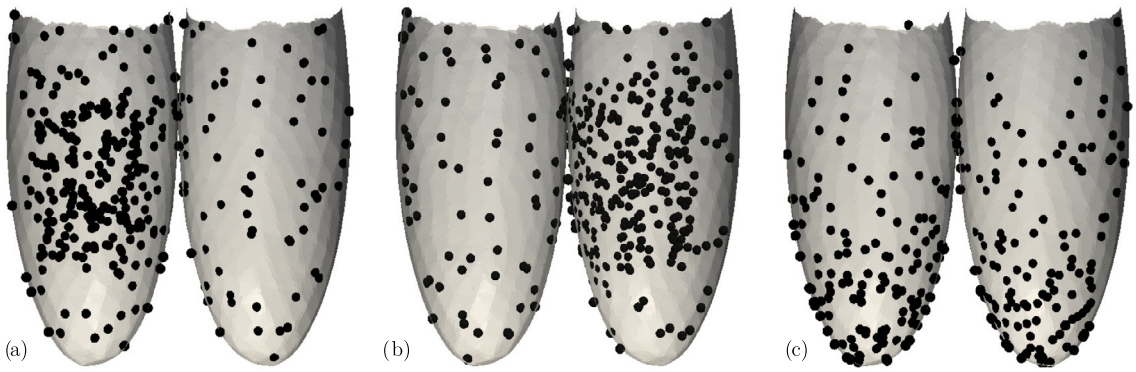

Fig. 8. Representation of the unbalanced samples' distributions on the two halves of the ventricle. (a) Unbalanced distribution on the septum; (b) unbalanced distribution on the opposite site of the septum; (c) unbalanced distribution on the apex. Unbalanced samples' distribution, idealized geometry.

Table 5
Mean absolute error E given by (28) and standard deviation σ given by (29) (in ms) for the patient-specific Purkinje networks generated with three different samples' distribution and for the related tentative networks. For each row, the name indicates the region where the measures were localized. Unbalanced samples' distribution, idealized geometry.

Region of unbalanced measures	Tentative	Patient specific
Septum	3.36 ± 3.12	1.71 ± 1.83
Opposite to the septum	3.48 ± 2.87	2.07 ± 1.95
Apex	4.03 ± 2.60	1.92 ± 1.86

Table 6
Mean absolute error E given by (28) and standard deviation σ given by (29) (in ms) for the tentative and the patient-specific Purkinje networks, for different values of the endocardial velocity V_e. Dependence of the accuracy on the endocardial velocity, idealized geometry.

Network/V_e	0.032 m/s	0.036 m/s	0.040 m/s
Tentative	3.67 ± 2.93	3.38 ± 2.76	3.76 ± 3.01
Patient-specific	3.06 ± 2.72	2.75 ± 2.64	3.02 ± 2.73

or when they are interested on the activation times in a specific region. To this aim, we considered three unbalanced distributions of the synthetic data, each of them characterized by a greater density of the measures in a specific region of the endocardium. In particular, we tested the algorithm with the following samples' configurations:

(i) Unbalanced distribution on the septum with $N = 324$ measures (see Fig. 8a);
(ii) Unbalanced distribution on the opposite site of the septum with $N = 366$ measures (see Fig. 8b);
(iii) Unbalanced distribution on the apex with $N = 283$ measures (see Fig. 8c).

The best value of the conduction velocity has been found to be $V_e = 0.35$ m/s for case (a) and $V_e = 0.36$ m/s for cases (b) and (c).

In Table 5 we reported the mean absolute error and the standard deviation obtained by the patient-specific Purkinje networks generated by using the three different samples' distributions, using the same tentative network as starting point.

From these results, we found for all the cases more or less the same accuracy when using the patient-specific network. We highlight that in any case the accuracy has been increased with respect to that obtained by using the tentative network. This showed that our method should be reliable also in real cases, when the measures are not acquired uniformly, independently of the region where they are localized.

4.6. Dependence of the solution on the choice of the endocardial velocity V_e

In this section we aim to study how the accuracy depends on the choice of the endocardial velocity V_e, which has been chosen with a trial-and-error strategy. To this aim, we re-ran the experiment reported in Section 4.4 with $N = 300$ points in the testing set, with two different values of V_e, namely $V_e = 0.032$ m/s and $V_e = 0.040$ m/s, the optimal values being $V_e = 0.036$ m/s.

In Table 6 we reported the mean absolute error and the standard deviation for the tentative and patient-specific networks, obtained for the three values of V_e. From these results we observe that a change of about 10% in the value of V_e produced an increase of the error of about 10% for both the patient-specific and the tentative networks.

Table 7
Mean absolute error E given by (28) and standard deviation σ given by (29) (in ms) obtained for different values of ω. The generation of the network has been driven by the sample $\widetilde{\mathcal{S}}(\omega)$, whilst their accuracy has been evaluated with respect to the sample $\mathcal{S}$. Noisy data, idealized geometry.

Network	ω	$E \pm \sigma$
Tentative	–	4.33 ± 3.05
Patient specific	0.00	1.64 ± 1.99
	0.05	1.87 ± 2.50
	0.10	1.81 ± 2.10
	0.20	2.42 ± 2.35

4.7. Accuracy in the case of noisy data

In order to mimic the measurement error introduced by the acquisition procedure, in this section we considered synthetic data affected by noise to generate the patient-specific network. To this aim, we considered a sample of synthetic data $\mathcal{S}$ composed by $N = 150$ measurements well-distributed on the endocardium and we added a random noise as follows:

$$\widetilde{T}_i = T_i + \omega \max_{i=1,\dots,N} \{|T_i|\} \mathcal{U}_{i[-0.5,0.5]} \quad i = 1, \dots, N, \tag{36}$$

where $\mathcal{U}_{i[-0.5,0.5]}$ is the uniform probability distribution in the interval $[-0.5, 0.5]$, and ω is the percentage of error. In this way, we obtained the "noisy" sample $\widetilde{\mathcal{S}}(\omega) := \{(\boldsymbol{x}_1, \widetilde{T}_1), \dots, (\boldsymbol{x}_N, \widetilde{T}_N)\}$ which has been then used to generate the patient-specific network. Of course, the accuracy of the generated network has been then evaluated with respect to the original sample $\mathcal{S}$.

In Table 7 we reported the mean absolute error and the standard deviation obtained by using the tentative and the patient-specific Purkinje network.

As expected, we found a decreased accuracy of the patient-specific network for increasing values of the noise. However, we still observed an excellent accuracy for $\omega = 0.05$ and $\omega = 0.1$. In any case, the mean absolute error was better than those obtained with the tentative network, also in the case $\omega = 0.2$. These results highlighted the robustness and accuracy of our method also in the presence of noisy data, justifying the effort needed to generate a patient-specific network.

5. Application to a real case

In this section we present two applications of the proposed method to a real geometry reconstructed starting from Magnetic Resonance Images (MRI). In the first one we generated synthetic data (see Section 4.2) to simulate the presence of a myocardial ischemia, whereas in the second one we considered real clinical data related to a normal propagation. The 3D geometry has been manually segmented from the MRI data and it has been discretized in a tetrahedral mesh composed of about $2.85 \cdot 10^5$ vertices and $1.5 \cdot 10^6$ elements.

5.1. Simulating an ischemic case

As observed, our method is not only valid in the case of a normal electrical propagation. Indeed, the only requirement for its validity is that the sources for the muscular activation are all located on the endocardium. Therefore, our method is still valid for a case characterized by a normal propagation in the network, with the presence of a myocardial ischemia in the muscle, that is a region characterized by reduced blood supply, resulting in the death of the muscular cells and thus in a progressive deterioration of the electrical activity (see [32] for a computational study).

Since we did not have real clinical data for the patient at hand related to a myocardial ischemia, we generated synthetic data by solving the 3D Eikonal problem (1) with a reference Purkinje network, as done for the idealized geometry in Section 4.2. Again, the reference network has been built with a different realization of the procedure used to generate the tentative network. In this way, the synthetic data $\mathcal{S} := \{(\boldsymbol{x}_1, T_1), \dots, (\boldsymbol{x}_N, T_N)\}$ were obtained by sampling $N = 150$ points on the endocardium with the exception of the ischemic region $\mathcal{I}$. Indeed, in this region the myocardium is no longer excitable, and accordingly we set

$$V_m(\boldsymbol{x}) = \begin{cases} 0.65 \text{ m/s}, & \text{if } x \notin \mathcal{I}, \\ 0.00 \text{ m/s}, & \text{if } x \in \mathcal{I}, \end{cases} \tag{37}$$

whereas we assumed that the portion of the Purkinje network belonging to that region is characterized by a reduced conduction velocity, since also the cells of the network are supposed to die under the reduced blood supply. In particular, we set

$$V_p(\boldsymbol{x}) = \begin{cases} 3.90 \text{ m/s}, & \text{if } x \notin \mathcal{I}, \\ 0.39 \text{ m/s}, & \text{if } x \in \mathcal{I}. \end{cases} \tag{38}$$

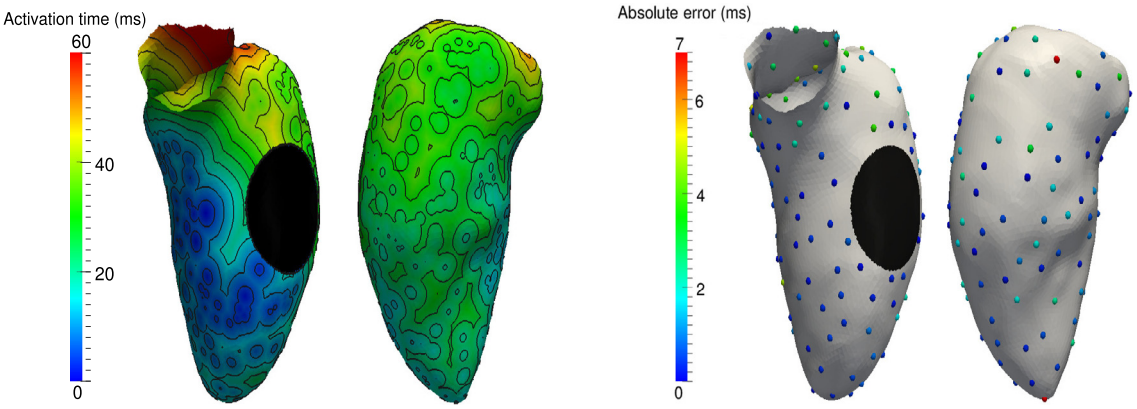

Fig. 9. Left: activation maps on the endocardium using the patient-specific Purkinje network generated by using synthetic measures; right: absolute error at the measurement points. Case with ischemia, real geometry, synthetic data.

Since we generated synthetically the measures, in this consistency test we assumed, for the sake of simplicity, an isotropic propagation through the myocardium. This corresponds to set $k = 1$ (and then $D = I$) for the solution of (1). In this case, since the propagation is isotropic, it is reasonable to assume that the velocity on the endocardium is equal to the one in the myocardium ($V_e = V_m$), so that no optimization on V_e was needed.

We then apply the proposed method for the generation of the patient-specific network by using the synthetic data, supposing to know the location of the ischemic region and thus the conduction velocities V_m and V_p in (37)–(38). Again, to validate our methodology, we computed the error (28) at the measurement points and the related standard deviations (29). We found $E = 1.30$ ms, $\sigma = 1.51$ ms for the patient-specific network, and $E = 3.37$ ms, $\sigma = 2.61$ ms for the tentative network. The numerical results also showed that 88.6% of the measures were satisfied when using the patient-specific network (34.0% for the tentative one). In Fig. 9 we depicted the simulated activation maps obtained by solving problem (1) with the generated patient-specific network, and the absolute errors at the measurement points.

This consistency test proved the reliability of the proposed method in the case of the presence of an ischemic region. Of course, a validation performed with real data of such a pathology will be mandatory. This is under study and it will be the subject of future works.

5.2. Clinical data related to a normal propagation

In the second real application we considered a case characterized by a normal propagation, where patient-specific clinical data have been used to generate the Purkinje network. In particular, the related activation times on the endocardium were acquired with the EnSite NavX system at the Division of Cardiology of Ospedale S. Maria del Carmine, Rovereto (TN), Italy, see [29] for more details.

In this case, since we have to face clinical measures, it was necessary to include the muscular fibers in our geometry in order to obtain physiological results. To this aim we used the strategy proposed in [20] which produces a uniform transmural variation of the direction of the fibers. This method is based on selecting three orthogonal directions for each point, the first one obtained by solving a harmonic problem and the second one aligned with the longitudinal ventricular axis.

The values used for the conduction velocities are: $V_p = 3.5$ m/s for the Purkinje network both to run our algorithm and for the final simulation, and $V_m = 0.98$ m/s for the velocity along the muscular fibers, whereas we set $k = 0.5$ for the ratio between the velocity orthogonal to the muscular fibers direction and that along the fibers. Moreover, we imposed the following boundary conditions for the fibers angle in the harmonic problem used to generate the muscular fibers: $-75°$ on the endocardium and $45°$ on the epicardium. As usual the value of the endocardial velocity used in our algorithm has been set with a trial-and-error strategy so as to maximize the accordance with the measures. In particular, we set $V_e = 0.6$ m/s.

We divided our measures in two groups, the training set used to generate the Purkinje network and the testing set used for the validation. We considered half of the measures in the testing set and the remaining measures in the training set. In Fig. 10 we represent the muscular fibers' direction, the tentative and the patient-specific Purkinje networks. We notice that our algorithm deleted some of the leaves and PMJ at the base of the ventricle. Probably, accordingly to the physiological knowledge, the Purkinje network is absent in this region, so that the clinical measures acquired in this region were related to points activated by the muscular propagation. Therefore, the activation in these points due to the tentative network was always early, and thus the related PMJ were deleted by our algorithm.

Moreover, we observe a qualitative analogy with the Purkinje networks of rabbits' hearts reconstructed with a micro-CT technique, see [26]. In particular, notice the absence of Purkinje fibers at the base of the ventricle and in the upper part of the septum, and the fractal structure of the network.

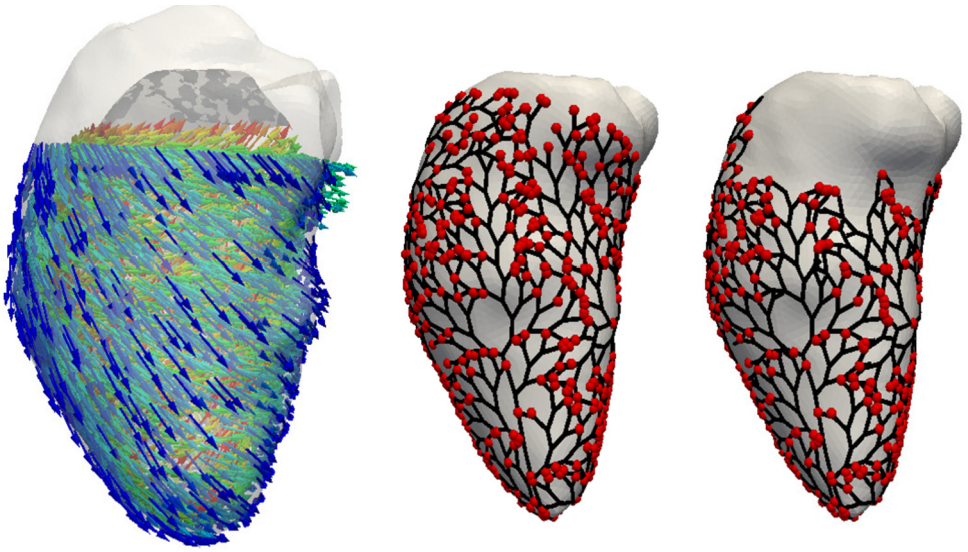

Fig. 10. Muscular fibers direction represented on a portion of the myocardium (left), tentative (middle), and patient-specific Purkinje network generated from clinical data (right). The PMJ are represented by the red spheres. Normal propagation, real geometry and data. (For interpretation of the references to color in this figure legend, the reader is referred to the web version of this article.)

In Fig. 11 we showed the contour lines of the activation maps obtained by solving problem (1) with the patient-specific network generated by our algorithm and the absolute errors in the measurements points of the testing set.

We found the following values for the mean absolute error and standard deviation given by (28) and (29): $E = 7.13 \pm 4.47$ ms for the tentative network and $E = 5.84 \pm 4.45$ ms for the patient-specific network. This highlights the improvement of the accuracy in the endocardium when using the patient-specific network. To perform a quantitative validation also in the myocardium one needs to have at disposal some measures also below the endocardium. However, the acquisition of the activation times in the myocardium is not a common procedure nowadays in the clinical practice.

6. Conclusions

In this work we proposed a new method for the generation of a patient-specific Purkinje network driven by clinical measures of the activation times on the endocardium. In particular, we considered the case of sources for the muscular activation all located on the endocardium, as happens, for example, for a normal electrical activity or for an ischemic case.

Our algorithm was based on the correction of a tentative network, generated by using a fractal law as proposed in [1, 12,21], improving the accordance with the measures. Its implementation is very simple and its efficiency very high since it requires the solution of 2D isotropic Eikonal problems on the endocardium, thus avoiding the knowledge of the muscular fibers and the computation in all the myocardium.

In the case of an ideal geometry and synthetic data, our numerical results highlighted:

1. The consistency of our method and the robustness with respect to the (randomly generated) tentative network;
2. The accuracy of our method when a cross-validation test was performed;
3. The robustness of our method when unbalanced or noisy data were considered;
4. A better accuracy in all the cases with respect to the one obtained with the tentative network.

Moreover, the numerical experiments performed in a real geometry highlighted:

5. The accuracy of our method when an ischemic region characterized by a vanishing conduction velocity was considered to generate synthetic data.
6. The accuracy of our method when applied to a real geometry with patient-specific measures related to a normal propagation.

For all these reasons, we believe that the proposed method could be an effective tool to improve the accuracy of the numerical results in computational electrocardiology.

We point out that the accuracy of our method to real cases characterized by a normal propagation has been already discussed in [29], whereas in [17] we have extended and applied our strategy to pathological cases, in particular to those cases where the muscular sources are not all located on the endocardium, such as in the Wolff–Parkinson–White syndrome. Other possible perspectives will be:

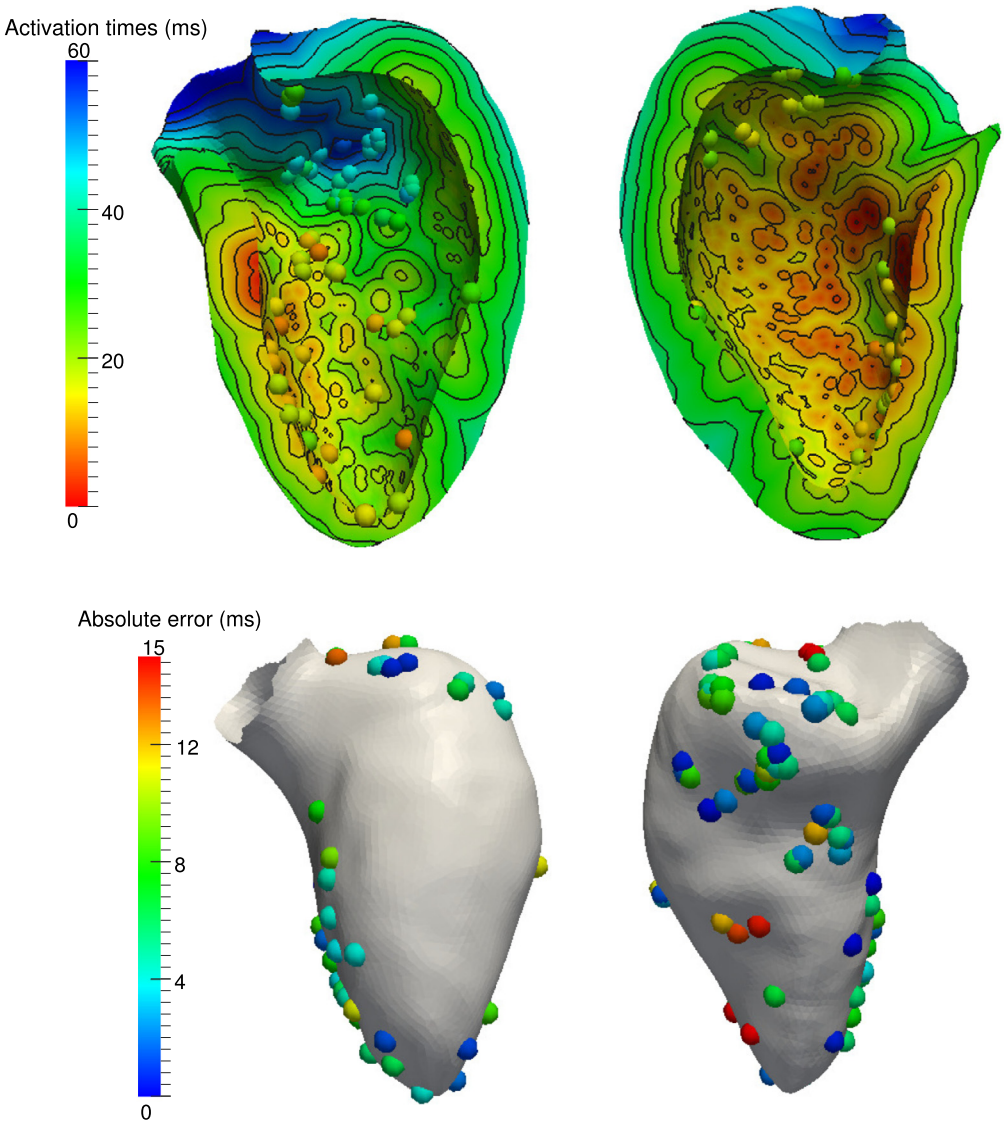

Fig. 11. Top: activation maps obtained by solving the 3D anisotropic Eikonal problem in the real geometry with the patient-specific Purkinje network and values of the measures in the testing set represented by bullets; bottom: absolute errors in the measurement points of the testing set. Normal propagation, real geometry and data.

- The extension of our method to the case where more accurate models, such as the Bidomain one, will be considered to compute the ventricular electrical activity;
- The application of our strategy to the Cardiac Resynchronization Therapy, for the optimization of the catheters stimulation.

Acknowledgements

The present study has been funded by “Fondazione Cassa di Risparmio di Trento e Rovereto” (CARITRO) within the project “Numerical modelling of the electrical activity of the heart for the study of the ventricular dyssynchrony”. The authors would like to thank M. Centonze and D. Catanzariti for having provided the radiological images and the electrical activation data.

References

[1] S. Abboud, O. Berenfeld, D. Sadeh, Simulation of high-resolution QRS complex using a ventricular model with a fractal conduction system. Effects of ischemia on high-frequency QRS potentials, Circ. Res. 68 (6) (1991) 1751–1760.

[2] R. Anderson, J. Yanni, M. Boyett, N. Chandler, H. Dobrzynski, The anatomy of the cardiac conduction system, Clin. Anat. 22 (1) (2009) 99–113.

[3] O. Berenfeld, J. Jalife, Purkinje-muscle reentry as a mechanism of polymorphic ventricular arrhythmias in a 3-dimensional model of the ventricles, Circ. Res. 2 (10) (1998) 1063–1077.
[4] R. Bordas, K. Gillow, Q. Lou, I. Efimov, D. Gavaghan, P.Kohl, V. Grau, B. Rodriguez, Rabbit-specific ventricular model of cardiac electrophysiological function including specialized conduction system, Prog. Biophys. Mol. Biol. 107 (1) (2011) 90–100.
[5] P. Chinchapatnam, K. Rhode, M. Ginks, C. Rinaldi, P. Lambiase, S.A.R. Razavi, M. Sermesant, Model-based imaging of cardiac apparent conductivity and local conduction velocity for diagnosis and planning of therapy, IEEE Trans. Med. Imaging 27 (2008) 1631–1642.
[6] R. Clayton, E. Cherry, O. Bernus, H. Dierckx, F. Fenton, L. Mirabella, A. Panfilov, F. Sachse, G. Seemann, H. Zhang, Models of cardiac tissue electrophysiology: progress, challenges and open questions, Prog. Biophys. Mol. Biol. 104 (1–3) (2011) 22–48.
[7] P. Colli Franzone, L. Guerri, Spreading excitation in 3-d models of the anisotropic cardiac tissue, I. Validation of the Eikonal model, Math. Biosci. 113 (1993) 145–209.
[8] P. Colli Franzone, L. Guerri, M. Pennacchio, B. Taccardi, Spreading excitation in 3-d models of the anisotropic cardiac tissue, II. Effects of the fiber architecture and ventricular geometry, Math. Biosci. 147 (1998) 131–171.
[9] P. Colli Franzone, L. Pavarino, A parallel solver for reaction–diffusion systems in computational electrocardiology, Math. Models Methods Appl. Sci. 14 (06) (2004) 883–911.
[10] D. Durrer, R. van Dam, G. Freud, M. Janse, F. Meijler, R. Arzbaecher, Total excitation of the isolated human heart, Circulation 41 (6) (1970) 899–912.
[11] D.J. Huelsing, K.W. Spitzer, J.M. Cordeiro, A.E. Pollard, Conduction between isolated rabbit Purkinje and ventricular myocytes coupled by a variable resistance, Am. J. Physiol., Heart Circ. Physiol. 274 (1998) H1163–H1173.
[12] T. Ijiri, T. Ashihara, T.Yamaguchi, K. Takayama, T. Igarashi, T. Shimada, T.Namba, R. Haraguchi, K. Nakazawa, A procedural method for modeling the Purkinje fibers of the heart, J. Physiol. Sci. 58 (7) (2008) 90–100.
[13] J. Keener, An eikonal-curvature equation for action potential propagation in myocardium, J. Math. Biol. 29 (7) (1991) 629–651.
[14] J. Keener, K. Bogar, A numerical method for the solution of the bidomain equations in cardiac tissue, Chaos 8 (1) (1998) 234–241.
[15] B. Kerckoffs, O. Faris, P. Boveenderd, F. Prinzen, K. Smits, T. Arts, Timing of depolarization and contraction in the paced canine left ventricle, J. Cardiovasc. Electrophysiol. 14 (2003) S188–S195.
[16] E. Konukoglu, M. Sermesant, O. Clatz, J. Peyrat, H. Delingette, N. Ayache, A recursive anisotropic fast marching approach to reaction diffusion equation: application to tumor growth modeling, in: IPMI 2007, in: Lect. Notes Comput. Sci., vol. 4584, Springer-Verlag, Berlin, Heidelberg, 2007, pp. 687–699.
[17] S. Palamara, C. Vergara, D. Catanzariti, E. Faggiano, M. Centonze, C. Pangrazzi, M. Maines, A. Quarteroni, Computational generation of the Purkinje network driven by clinical measurements: the case of pathological propagations, Int. J. Numer. Methods Biomed. Eng. 30 (12) (2014) 1558–1577.
[18] D. Rawling, R. Joyner, E. Overholt, Variations in the functional electrical coupling between the subendocardial Purkinje and ventricular layers of the canine left ventricle, Circ. Res. 57 (2) (1985) 252–261.
[19] D. Romero, R. Sebastian, B.H. Bijnens, V. Zimmerman, P.M. Boyle, E.J. Vigmond, A.F. Frangi, Effects of the Purkinje system and cardiac geometry on biventricular pacing: a model study, Ann. Biomed. Eng. 38 (2010) 1388–1398.
[20] S. Rossi, T. Lassila, R. Ruiz-Baier, A. Sequeira, A. Quarteroni, Thermodynamically consistent orthotropic activation model capturing ventricular systolic wall thickening in cardiac electromechanics, Eur. J. Mech. A, Solids 48 (2014) 129–142.
[21] R. Sebastian, V. Zimmerman, D. Romero, A. Frangi, Construction of a computational anatomical model of the peripheral cardiac conduction system, Prog. Biophys. Mol. Biol. 58 (12) (2011) 90–100.
[22] R. Sebastian, V. Zimmerman, D. Romero, D. Sanchez-Quintana, A.F. Frangi, Characterization and modeling of the peripheral cardiac conduction system, IEEE Trans. Med. Imaging 32 (2013) 45–55.
[23] M. Sermesant, R. Chabiniok, P. Chinchapatnam, T. Mansi, F. Billet, P. Moireau, J. Peyrat, K. Wong, J. Relan, K. Rhode, M. Ginks, P. Lambiase, H. Delingette, M. Sorine, C. Rinaldi, D. Chapelle, R. Razavi, N. Ayache, Patient-specific electromechanical models of the heart for the prediction of pacing acute effects in CRT: a preliminary clinical validation, Med. Image Anal. 16 (1) (2012) 201–215.
[24] J.A. Sethian, Fast marching methods, SIAM Rev. 41 (2) (1999) 199–235.
[25] J.A. Sethian, A. Vladimirsky, Ordered upwind methods for static Hamilton–Jacobi equations: theory and algorithms, SIAM J. Numer. Anal. 41 (1) (2003) 325–363.
[26] R. Stephenson, M. Boyett, G. Hart, T. Nikolaidou, X. Cai, A. Corno, N. Alphonso, N. Jeffery, J. Jarvis, Contrast enhanced micro-computed tomography resolves the 3-dimensional morphology of the cardiac conduction system in mammalian hearts, PLoS ONE 7 (4) (2012) e35299.
[27] C. Tobon-Gomez, N. Duchateau, R. Sebastian, S. Marchesseau, O. Camara, E. Donal, M.D. Craene, A. Pashaei, J. Relan, M. Steghofer, P. Lamata, H. Delingette, S. Duckett, M. Garreau, A. Hernandez, K. Rhode, M. Sermesant, N. Ayache, C. Leclercq, R. Razavi, N. Smith, A. Frangi, Understanding the mechanisms amenable to CRT response: from pre-operative multimodal image data to patient-specific computational models, Med. Biol. Eng. Comput. (2013), http://dx.doi.org/10.1007/s11517-013-1044-7.
[28] K. Tusscher, A. Panfilov, Modelling of the ventricular conduction system, Prog. Biophys. Mol. Biol. 96 (1–3) (2008) 152–170.
[29] C. Vergara, S. Palamara, D. Catanzariti, C. Pangrazzi, F.Nobile, M. Centonze, E. Faggiano, M. Maines, A. Quarteroni, G. Vergara, Patient-specific generation of the Purkinje network driven by clinical measurements of a normal propagation, Med. Biol. Eng. Comput. 52 (10) (2014) 813–826.
[30] E. Vigmond, F. Aguel, N. Trayanova, Computational techniques for solving the bidomain equations in three dimensions, IEEE Trans. Biomed. Eng. 49 (11) (2002) 1260–1269.
[31] E. Vigmond, C. Clements, Construction of a computer model to investigate sawtooth effects in the Purkinje system, IEEE Trans. Biomed. Eng. 54 (3) (2007) 389–399.
[32] D. Wang, R. Kirby, R. MacLeod, C. Johnson, Inverse electrocardiographic source localization of ischemia: an optimization framework and finite element solution, J. Comput. Phys. 250 (2013) 403–424.